Inorganic Chemistry

Article

pubs.acs.org/IC

Electrons per Atom Ratio Determination and Hume-Rothery Electron Concentration Rule for P-Based Polar Compounds Studied by FLAPW−Fourier Calculations

Uichiro Mizutani,*[,†] Hirokazu Sato,[‡] Manabu Inukai,[§] Yoichi Nishino,[§] and Eeuwe Sieds Zijlstra[∥]

[†]Nagoya Industrial Science Research Institute, 1-13 Yotsuya-dori, Chikusa-ku, Nagoya 464-0819, Japan

[‡]Aichi University of Education, Kariya-shi, Aichi 448-8542, Japan

[§]Department of Frontier Materials, Nagoya Institute of Technology, Gokiso-cho, Showa-ku, Nagoya 466-8555, Japan

[∥]Theoretical Physics, University of Kassel, 34132 Kassel, Germany

ABSTRACT: The extent to which reliable electrons per atom ratio, e/a, are determined and the validity of the Hume-Rothery stabilization mechanism are ensured upon increasing ionicity are studied by applying first-principles full potential linearized augmented plane wave (FLAPW)−Fourier band calculations to as many as 59 binary compounds formed by adding elements from periods 2−6 to phosphorus in group 15 of the Periodic Table. Van Arkel-Ketelaar triangle maps were constructed both by using the Allen electronegativity data and by using an energy difference between the center-of-gravity energies of FLAPW-derived s and p partial densities of states (DOSs) for the equiatomic compounds studied. The determination of e/a and the test of the interference condition, both of which play a key role in the Hume-Rothery stabilization mechanism, were reliably made for all intermetallic compounds, as long as the ionicity is less than 50%. In the A−P (A = Li, Na, K, Rb, and Cs) compounds with ionicity exceeding 50%, however, e/a determination becomes unstable, as reflected in its P concentration dependence. New Hume-Rothery electron concentration rules were theoretically found in two families of polar compounds: skutterudite compounds TMP_3, $TMAs_3$, and $TMSb_3$ (TM = Co, Ni, Rh, and Ir; cI32) with e/a = 4.34 and TM_3P (TM = Cr, Mn, Fe, and Ni; tI32) with e/a = 2.20.

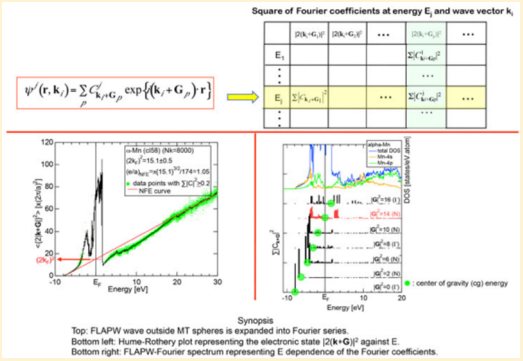

1. INTRODUCTION

The Hume-Rothery electron concentration rule was empirically established in the 1920−1930s in noble metals alloyed with polyvalent elements located to their right in the Periodic Table through extensive efforts by contemporary researchers including the metallurgist Hume-Rothery in England and the powder X-ray diffraction crystallographers Westgren and Phragmén in Sweden.[1−7] In 1936, Mott and Jones[8] laid its theoretical foundation within the framework of the free-electron model and claimed that the *critical* electron concentration denoted as e/a, or the number of free electrons per atom, is determined from the condition that a spherical Fermi surface touches the Brillouin zone of relevant phases. Their theory was so simple and transparent that it has been taken as one of the greatest achievements in the history of the electron theory of metals.

Since then, we have gradually built up a general consensus such that alloys or compounds obeying the Hume-Rothery electron concentration rule are restricted only to those in which the electronic structure can be described within the nearly free-electron (NFE) model and discussed in terms of the interaction of the Fermi surface with the Brillouin zone. Great surprise and confusion had arisen in the early 1990s when Tsai and his co-workers discovered a series of thermally stable quasicrystals in Al−Cu−TM (TM = Fe, Ru, and Os) and Al−Pd−TM (TM = Mn and Re) alloy systems, where TM is a transition metal, by using the Hume-Rothery electron concentration rule as a guide.[9−12] This is because no one had expected the Hume-Rothery electron concentration rule to hold in TM-bearing compounds, where orbital hybridization effects are so substantial that the NFE model, on which Mott and Jones relied, definitely fails. Strong suspicions were also aroused by their choice of negative e/a values originally proposed by Raynor in 1949[13] for the TM 3d elements. This is because Raynor postulated negative e/a values for elements from Cr to Ni on the basis of the Pauling model in 1938,[14] which was obviously too crude to produce any reliable numerical data. We consider the most important message conveyed by Tsai[12] to be found in his finding that the values of e/a are kept constant, regardless of the choice of atomic species of TM elements in a given group of the Periodic Table, say, Fe, Ru, and Os in the Al−Cu−TM alloy system. This must be the greatest outcome experimentally drawn and certainly deserves theoretical studies to elucidate the physics behind it. Instead, its numerical figure

Special Issue: To Honor the Memory of Prof. John D. Corbett

Received: September 24, 2014
Published: December 22, 2014

   dx.doi.org/10.1021/ic502286q | *Inorg. Chem.* 2015, 54, 930−946

of e/a, i.e., e/a = 1.8 for the MI-type quasicrystals obtained by using Raynor's negative e/a values for the TM elements, is, we believe, arbitrary.

During the period from the early 1990s to the early 2000s, the origin of a pseudogap at the Fermi level in the 1/1−1/1−1/1 approximants, the counterpart to the MI-type quasicrystals, had been almost exclusively discussed in terms of orbital hybridization effects within the framework of linearized muffin-tin orbital atomic sphere approximation (LMTO-ASA) band calculations. Unfortunately, the approach along this line[15−17] was not suited to extract e/a-dependent quantities such as the interference condition satisfied by electrons at the Fermi level interacting with particular Brillouin zones and e/a itself. As a consequence, no theoretical interpretation had been advanced to explain why the e/a-dependent phase stabilization mechanism or the Hume-Rothery electron concentration rule works in MI-type quasicrystals and their approximants, as proposed by Tsai in an empirical way.[12]

A breakthrough has been brought about in the past decade by Mizutani and co-workers,[7,18−28] who developed a method that makes full use of the first-principles full-potential linearized augmented plane wave (FLAPW) formalism: the wave function is expressed in the form of the radial wave function times the spherical harmonics inside the muffin-tin (MT) spheres, while it is expanded into the Fourier series, i.e., the superposition of plane waves over allowed reciprocal lattice vectors $\mathbf{G}_p$ outside the MT spheres. Note that the d states in the TM elements having a highly localized tendency around the nucleus tend to be confined within the MT spheres. The gist of the new method is to focus on the wave function outside the MT spheres, from which the Fermi surface−Brillouin zone interaction can be extracted even in TM-bearing compounds substantially involving d states in the valence band.

In detail, the dispersion relation is constructed for electrons outside the MT spheres, from which the diameter of the effective Fermi sphere, $(2k_F)^2$, and the number of itinerant electrons per atom, e/a, are easily deduced. This is referred to as the Hume-Rothery plot. The energy dependence of the square of the Fourier coefficient, $\sum|C^j_{\mathbf{k}_i+\mathbf{G}_p}|^2$, for the $|\mathbf{G}|^2$-specified plane waves at a particular symmetry point of the Brillouin zone is called the FLAPW−Fourier spectrum, where $\mathbf{k}_i + \mathbf{G}_p$ is replaced by another reciprocal lattice vector $\mathbf{G}$ (the summation is taken under the condition $|\mathbf{k}_i + \mathbf{G}_p|$ = constant).[24] The center-of-gravity (CG) energy is calculated by taking a CG of the Fourier coefficients for each $|\mathbf{G}|^2$-specified energy spectrum. From the $|\mathbf{G}|^2$ dependence of CG energies, one can easily extract its *critical* one at the Fermi level. This is equivalent to extraction of the Brillouin zone mostly interacting with electrons at the Fermi level. Hereafter, the $|\mathbf{G}|^2$ thus extracted is called *critical* and is denoted as $|\mathbf{G}|_c^2$. As will be described in detail later, a new method of taking the CG energy in both the FLAPW−Fourier spectrum and the Hume-Rothery plot in combination with the introduction of the so-called tetrahedron method has made it possible to more reliably and more consistently determine both $(2k_F)^2$ and e/a from the Hume-Rothery plot and $|\mathbf{G}|_c^2$ from the FLAPW−Fourier spectrum for intermetallic compounds containing a large amount of TM elements.[19,24]

We are now ready to review some of the major results derived from the FLAPW−Fourier analysis for structurally complex metallic alloys (CMAs) including MI-type 1/1−1/1−1/1 approximants Al−Mn, Al−Re, and Al−Cu−Fe−Si.[7,18−28] The three electronic parameters $(2k_F)^2$, e/a, and $|\mathbf{G}|_c^2$ were determined for each CMA and were employed to test whether the interference condition is satisfied. The confirmation of the validity of the interference condition for a large number of pseudogap-bearing CMAs led to the conclusion that the e/a-dependent or Hume-Rothery stabilization mechanism holds even in systems where the departure from free-electron behavior is substantial because of strong orbital hybridization in Al−TM-based CMAs including MI-type approximants. The e/a values for TM 3d, 4d, and 5d elements along with their neighboring elements have also been determined.[24,25]

The e/a values for the MI-type quasicrystals were easily estimated by taking the composition average of the e/a values of their constituent elements: $(e/a)_{Al}$ = 3.0, $(e/a)_{Mn}$ = 1.05, $(e/a)_{Fe}$ = 1.05, $(e/a)_{Cu}$ = 1.0, etc.[20,24] It is found that e/a for $Al_{63}Cu_{25}TM_{12}$ (M = Fe, Ru, and Os) and $Al_{70}Pd_{20}TM_{10}$ (TM = Mn and Re) quasicrystals is centered at 2.2,[20,24] in disagreement with e/a = 1.8 postulated by Tsai,[12] who employed negative e/a for the TM elements. A shift of e/a to 2.2 is certainly due to the assignment of positive e/a values for these TM elements. The most important message is not to point out a disagreement in the numerical figure of e/a but the theoretical proof for the validity of the e/a = constant rule even in CMAs containing a large amount of TM elements.

As is well-known, chemical types of bonds between atoms in alloys and compounds can be discussed in terms of the ionicity, metallicity, and covalency. As discussed above, it has now become clear that the applicability range of the Hume-Rothery stabilization mechanism is not limited only to a very narrow metallic regime, where the NFE model works, but covers a much wider range where both metallicity and covalency coexist like in the MI-type approximants. We are aware that the degree of ionicity also plays a key role in forming a solid. Polar compounds are characterized by the presence of a sizable charge transfer from an electropositive element to an electronegative one.

In 2013, Mizutani et al.[26] addressed the issue of whether the Hume-Rothery stabilization mechanism works and e/a can still be well-defined when the degree of ionicity is enhanced and attempted to determine the three key electronic parameters $(2k_F)^2$, e/a, and $|\mathbf{G}|_c^2$ for Zintl compounds AX (A = Li and Na and X = Al, Ga, In, and Tl), where a large amount of charge transfer is known to occur from the alkali metal to the trivalent element.[29]

The FLAPW−Fourier studies for the series of Zintl compounds mentioned above revealed that the pseudogap-bearing parabolic density of state (DOS) is modulated by many spiky peaks, which are reflected as kinks in an otherwise free-electron-like linear dispersion relation in the Hume-Rothery plot. It turned out that values of $(2k_F)^2$ and e/a are distributed around 16.0 ± 0.2 and 2.09 ± 0.06, respectively, which is in good agreement with e/a = 2.0 obtained by taking a composition average of mono- and trivalent elements for equiatomic Zintl compounds AX. Moreover, the value of $|\mathbf{G}|_c^2$ was determined to be 16 from the FLAPW−Fourier spectra without exception, confirming fulfillment of the interference condition. It was concluded that the Zintl compounds AX *do* obey the Hume-Rothery electron concentration rule and stabilization mechanism, even though they are known to be typical of polar intermetallics.[26]

In the present work, we will attempt to gain more comprehensive insight into the conditions under which the Hume-Rothery stabilization mechanism and electron concen-

dx.doi.org/10.1021/ic502286q | Inorg. Chem. 2015, 54, 930−946

tration rule remain valid or break down in polar intermetallic compounds, where the ionicity is increased at the expense of the metallicity and/or covalency. For this purpose, we have performed FLAPW–Fourier analysis for a large number of binary phosphorus compounds, where phosphorus is chosen as a highly electronegative element and is alloyed with elements in periods 2–6 of the Periodic Table, including all TM 3d elements from Sc to Cu. To quantify the degree of metallicity, ionicity, and covalency of the bonds in these compounds, we specifically constructed the so-called van Arkel–Ketelaar triangles,[30,31] which will be described in section 2. The FLAPW electronic structure calculations and the essence of the FLAPW–Fourier method employed in the present work will be discussed in section 3. To evaluate the degree of covalency and ionicity in the compounds that we studied, we newly employed a separation energy associated with the CG energy in the FLAPW-derived s and p partial DOSs for both pure elements and intermetallic compounds. Results and discussion will be given in section 4.

2. VAN ARKEL–KETELAAR TRIANGLE

The validity of the Hume-Rothery stabilization mechanism not just for almost free-electron-like systems but also for TM-bearing systems, where orbital hybridization effects are significant, has prompted us to study its bond-type dependence. We consider construction of the van Arkel–Ketelaar triangle to be helpful. An equilateral triangle with vertices designated as metallic (M), ionic (I), and covalent (C) allows us to locate any binary equiatomic compound at an explicit position inside the triangle.

According to Allen et al.,[30] the electronegativity (or configuration energy) for any element is defined as an average energy of the outermost electrons in its free atom:

$$\chi_{spec} = (n_s I_s + n_p I_p)/(n_s + n_p) \quad (1)$$

where n_s and n_p represent the number of s and p electrons in the outermost shell of the free atom and I_s and I_p are the corresponding ionization energies, respectively. In the case of TM elements, n_p and I_p are replaced by n_d and I_d, respectively. All parameters in eq 1 were accurately determined from spectroscopic measurements for free atoms in the ground state and are available with high accuracy from the National Bureau of Standard Tables.[31,32] The value of χ_{spec}, say, in elements in period 3, starts from the lowest value of 0.869 for Na and increases step by step with increasing atomic number up to 2.869 for Cl (the absolute values in electronvolts are multiplied by 0.169[31]). Clearly, an increase in χ_{spec} with increasing atomic number corresponds to a widening of the energy difference between s and p electron energy levels of the free atom.

If a given atom is surrounded by others, energy bands will be formed. The closer the free atom energy level spacings are, the more the energy band becomes free-electron-like. Also, in reverse, the wider the s and p free atom energy spacings are, the more isolated the s and p partial DOSs are. This means that an increase in Allen's electronegativity, say, from Na to Cl in period 3 of the Periodic Table, would result in the growth of covalency at the expense of metallicity. By extending the idea above, Allen et al.[30] proposed that the degrees of covalency and ionicity for an equiatomic binary compound consisting of elements A and B can be scaled in terms of an average of electronegativities χ^A_{spec} and χ^B_{spec} and its difference, respectively:

$$\chi_{AB} = (\chi^A_{spec} + \chi^B_{spec})/2 \quad (2)$$

and

$$\Delta\chi_{AB} = |\chi^A_{spec} - \chi^B_{spec}| \quad (3)$$

We are aware that body-centered-cubic (bcc) Na and orthorhombic Cl respectively possess the smallest and largest electronegativities among the elements in period 3 of the Periodic Table because the inert gas element Ar, for which the van der Waals force is responsible, is excluded. A core assumption in the Allen approach in construction of the van Arkel–Ketelaar triangle[30] is to treat Na, Cl, and NaCl as ideal substances and to force them to be located at coordinates (X, Y, Z) = (0, 0, 100), (100, 0, 0), and (0, 100, 0) on the vertices M, C, and I of the triangle, where X, Y, and Z are variables representing the degree of covalency, ionicity, and metallicity, respectively. The Allen electronegativity data for pure elements from Na to Cl in period 3 must fall on the side MC of the triangle because of the absence of ionicity originating from charge transfer between unlike constituent elements. Using the relation $X = a\chi_A + b$ (%), we can transfer the Allen data to an explicit position on the side MC of the triangle. The coefficients a and b are determined to be 50 and −43.45, respectively, under the constraints (χ_{Na}, X) = (0.869, 0) and (χ_{Cl}, X) = (2.869, 100).[30,31] The positions of all of the remaining elements Mg, Al, Si, P, and S in period 3 are immediately fixed on the side MC, as shown in Figure 1.

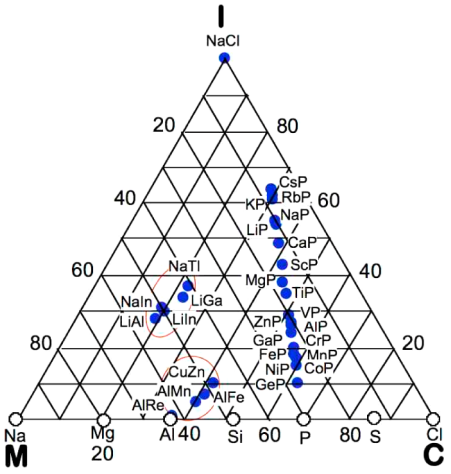

Figure 1. van Arkel–Ketelaar triangle constructed by inserting the Allen electronegativity data[30,31] into eqs 2 and 3 for 28 equiatomic compounds (blue solid circle) and seven elements (○) in period 3 of the Periodic Table. The equiatomic Zintl compounds AX (A = Li and Na and X = Al, Ga, In, and Tl) and Al–TM compounds are circled with red to distinguish them from the family of P-based compounds.

The data for the equiatomic compounds of our interest are added to Figure 1 by inserting the Allen electronegativity data into eqs 2 and 3. For consistency, the relationship $X = 50\chi_{AB} - 43.45$ discussed above for pure elements is used for the equiatomic compounds as well. A finite ionicity sets in from eq 3 when $\chi^A_{spec} \neq \chi^B_{spec}$, specifying the variable Y orthogonal to the side MC of the triangle. The relationship $Y = c\Delta\chi_{AB}$ (%) is employed to transfer $\Delta\chi_{AB}$ to the variable Y. The metallicity variable Z cannot be independently determined but is constrained by $Z = 100 - X - Y$ (%). Because NaCl should be located at the vertex I, the condition (Y, $\Delta\chi_{AB}$) = (100, 2.0)

dx.doi.org/10.1021/ic502286q | Inorg. Chem. 2015, 54, 930–946

immediately leads to the coefficient $c = 50$. We realized that $c = 50$ cannot be assumed for all of the equiatomic compounds because Z becomes negative in some compounds in which $X + Y$ happens to exceed 100. Thus, we have to reduce the coefficient c so as to confine all of the data points inside the triangle. In the present work, c is fixed at 40 for all of the equiatomic compounds except for NaCl. The results thus obtained are incorporated in Figure 1.

As can be seen from Figure 1, data points for a series of P-based equiatomic compounds fall on an almost vertical strip, with the highest ionicity of 64% for CsP. If $c = 35$ is used, the strip is shifted a few percentage points as a whole to a higher metallicity side at the expense of ionicity and the highest ionicity for CsP is lowered to 56%. In spite of such ambiguity, we judge that Figure 1 can be safely used to assess the degree of ionicity of a given compound relative to others in the family of P-based compounds because their relative positions remain unchanged, regardless of the choice of the value of the coefficient c.

At this stage, it may be worthwhile to mention the location of the insulators in Figure 1. Metallicity emerges as soon as we depart from the side CI of the triangle. This does not mean that all insulators are confined on the side CI. For example, the semiconductor Si, which has a finite energy gap at the Fermi level, is situated at the position (52, 0, 48) on the side MC. As is well-known, Si 3s and 3p electrons form a continuous valence band of 11.9 eV in width. A broad band itself is taken as the manifestation of its metallicity. As we go further to the right on the side MC, three more elements, P, S, and Cl, appear, where the valence band begins to split into many peaks associated with their s and p states. This is taken as an indication for the growth of covalency accompanying strong bond orientations in them.

As is clear from the argument above, one cannot uniquely separate the metallicity from the other two quantities in the van Arkel−Ketelaar triangle map. There is definitely some arbitrariness in the argument. For example, pure elements K and Br and compound KBr are also implicitly placed at vertices M, C, and I in Figure 1, respectively, without differentiating the Allen electronegativities between K ($\chi^{K}_{spec} = 0.734$) and Na ($\chi^{Na}_{spec} = 0.869$). Thus, the triangle should be used at a qualitative level. Moreover, we are encouraged from the studies above to investigate to what extent Allen's electronegativity can be used to assess the degree of bonds in solids because it is derived purely from the spectroscopic data of free atoms. In section 4, we will try to replace χ_{AB} and $\Delta\chi_{AB}$ by quantities derived directly from first-principles FLAPW band calculations for pure elements and compounds with the hope that some deeper insight into the character of interatomic bonds in alloys and compounds is gained.

3. ELECTRONIC STRUCTURE CALCULATIONS

3.1. *WIEN2k*−FLAPW Band Calculations and Structure Information. Briefly, the *WIEN2k* program package[33] was employed to perform the FLAPW electronic structure calculations, using two INTEL version personal computers [Linux OS, Ubuntu 10.04; CPU, Intel(R) Core(TM) i7-2700K 3.50 GHz; memory, DDR3 16 GB (1333 MHz); Fortran compiler, Intel Fortran 11.1.080 + MKL 11.1.080; compiler option, -openmp; environment variable, OMP_NUM_THREADS=8].

Structure information about binary compounds alloyed with P studied in the present work was collected from *Pearson's Handbook*.[34]

3.2. Total and Partial DOSs. The total and s, p, and d partial DOSs were calculated by executing the FLAPW band calculations for pure elements and all compounds studied. It is noted that partial DOSs are constructed from electrons inside the MT sphere. The CG (or cg) energy for occupied states is evaluated by integrating the s and p partial DOSs up to the Fermi level. A difference in the CG energies, $|E_{cg-s} - E_{cg-p}|$, between the s and p partial DOSs is calculated not only for elements but also for the constituent elements A and B in the equiatomic compounds AB. We consider $|E_{cg-s} - E_{cg-p}|$ to be worthy of testing as a substitute for the s and p energy level spacings of free atoms.

3.3. e/a Determination. In *WIEN2k*, the first Brillouin zone is partitioned into $N_{\mathbf{k}}$ cells, and the value of $\mathbf{k}_i$ is fixed at each corner, where i runs from 1 to $N_{\mathbf{k}}$. Solving the Schrödinger equation at any wave vector $\mathbf{k}_i$ results in a set of multivalued FLAPW wave functions and corresponding energy eigenvalues. Let us consider the jth wave function outside the MT spheres with the energy eigenvalue E^j at the wave vector $\mathbf{k}_i$. It is expressed as a Fourier series:

$$\psi^j(\mathbf{r}, \mathbf{k}_i) = \sum_p C^j_{\mathbf{k}_i+\mathbf{G}_p} \exp\{i(\mathbf{k}_i + \mathbf{G}_p)\cdot\mathbf{r}\} \tag{4}$$

where $\mathbf{G}_p$ is the allowed reciprocal lattice vector. We can now envision a matrix of the square of the Fourier coefficient $\sum|C^j_{\mathbf{k}_i+\mathbf{G}_p}|^2$ arranged in rows and columns with two variables j and p for each wave vector $\mathbf{k}_i$. The *Fortran* program then seeks the FLAPW state $\{2|\mathbf{k}_i + \mathbf{G}_p|\}_j^2$ having the largest Fourier coefficient for a given E_j and $\mathbf{k}_i$. This is done for all $\mathbf{k}_i$ values over the range $1 \le i \le N_{\mathbf{k}}$ in the first Brillouin zone in an energy interval $E_j \le E < E_j + \Delta E$, where E_j runs from the bottom of the valence band up to +30 eV above the Fermi level with an increment ΔE generally set as 0.05 eV for all systems studied. An average of $\{2|\mathbf{k}_i + \mathbf{G}_{p_0}|\}_E^2$ over $i = 1$ to $N_{\mathbf{k}}$ is now calculated by using the relationship

$$\langle\{2|\mathbf{k} + \mathbf{G}|\}^2\rangle_E = \frac{\sum_{i=1}^{N_{\mathbf{k}}} \omega_i\{2|\mathbf{k}_i + \mathbf{G}_{p_0}|\}_E^2}{\sum_{i=1}^{N_{\mathbf{k}}} \omega_i} \tag{5}$$

where ω_i represents degeneracies, including possibly zero, of the selected electronic states $\{2|\mathbf{k}_i + \mathbf{G}_{p_0}|\}_E^2$ in a given energy interval. The plot of $\langle\{2|\mathbf{k} + \mathbf{G}|\}^2\rangle_E$ versus E is called the Hume-Rothery plot and represents the energy dispersion relationship of electrons outside the MT spheres.

The tetrahedron (TH) method was introduced to substantially reduce the scatter of data points in the Hume-Rothery plot.[24] The resulting fairly smoothed HR curve has been referred to as TH−HR curve. As mentioned in the Introduction, the method of taking a CG energy was further introduced to circumvent the anomalies due to formation of an energy gap and also due to growth of a d band having a strongly localized tendency near the Fermi level. Its essence is briefly reviewed.

The CG energy $E^{cg}_{\mathbf{k}_i+\mathbf{G}_p}$ is calculated from the energy dependence of the Fourier coefficients in each column specified by $\mathbf{k}_i + \mathbf{G}_p$ in the matrix with a variable j:

dx.doi.org/10.1021/ic502286q | Inorg. Chem. 2015, 54, 930−946

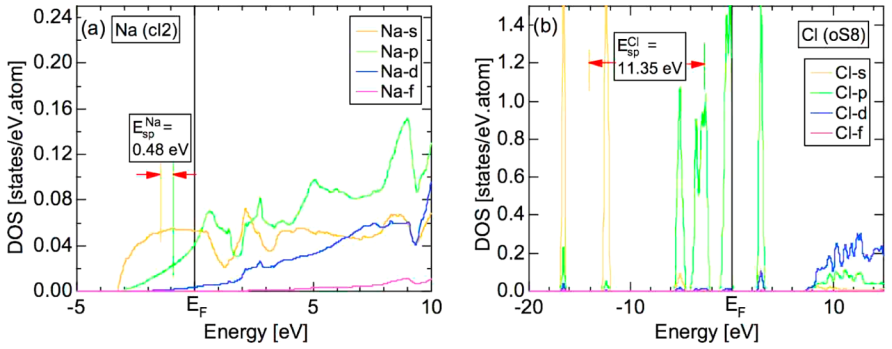

Figure 2. (a) Na partial DOSs and its separation energy E_{sp}^{Na} for bcc Na (cI2) and (b) Cl partial DOSs and its separation energy E_{sp}^{Cl} for orthorhombic Cl (oS8).

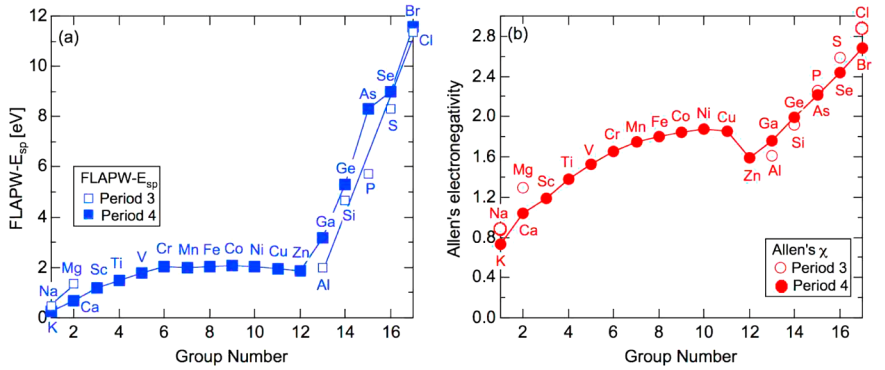

Figure 3. (a) FLAPW separation energy E_{sp} and (b) Allen electronegativity χ_{spec} for elements in periods 3 and 4 of the Periodic Table.

$$E^{cg}_{\mathbf{k}_i+\mathbf{G}_p} = \frac{\sum_j E_j(\mathbf{k}_i)|C^j_{\mathbf{k}_i+\mathbf{G}_p}|^2}{\sum_j |C^j_{\mathbf{k}_i+\mathbf{G}_p}|^2} \quad (6)$$

where $E^{cg}_{\mathbf{k}_i+\mathbf{G}_p}$ is calculated for each variable i and each p. To make the computation in an effective but reliable way, we retain the first L Fourier coefficients $\sum|C^j_{\mathbf{k}_i+\mathbf{G}_p}|^2$ for the jth wave function in descending order, and the rest is set to zero. To avoid any ambiguity in the present studies, the value of L is set to unity; i.e., we retain only the maximum Fourier coefficient.

In this way, the set of $\{2|\mathbf{k}_i + \mathbf{G}_p|\}^2$ and $E^{cg}_{\mathbf{k}_i+\mathbf{G}_p}$ data is produced and has been referred to as CG−HR data points. The TH method is then applied for CG−HR data points. The resulting smoothed HR curve is referred to as the CG−TH−HR curve or simply the NFE curve.[24] It can almost perfectly smooth out the anomaly due to energy gap formation in the TH−HR curve and allows us to accurately determine $(2k_F)^2$ and e/a for pure elements and intermetallic compounds with P.

Before ending this section, we direct our attention to a key issue regarding the criterion to judge when the CG−TH−HR curve has to be calculated. Obviously, we need the NFE approximation in a system, where electrons at the Fermi level deviate heavily from the free-electron behavior, say, because of the presence of a d band or the formation of energy gaps. This can be judged in several ways.[20,24] Among them, the most convenient criterion is based on the sum of the square of the Fourier coefficients, $\sum|C^j_{\mathbf{k}_i+\mathbf{G}_p}|^2$, of the jth wave function outside the MT spheres at a given state $\mathbf{k}_i$.[24] In the free-electron model, only a single Fourier coefficient remains finite at a particular $\mathbf{k}_i + \mathbf{G}_p$ for the jth wave function, and its value is essentially unity. In contrast, when electrons tend to be localized, the j-th wave function would naturally involve a number of Fourier coefficients comparable in magnitude. As a consequence, even the largest one would be suppressed, say, below 0.1. Our criterion is set in such a way that the NFE curve should be calculated, provided that electrons satisfying the condition $\sum|C^j_{\mathbf{k}_i+\mathbf{G}_p}|^2 \geq 0.2$ are scarcely found at the Fermi level. These data points marked with green dots are added to the Hume-Rothery plots. For example, green dots are obviously abundant at the Fermi level in Figures 6 and 7. In these cases, the value of $(2k_F)^2$ is determined by directly reading off the ordinate of the TH−HR data points at the Fermi level. This has been referred to as the "local reading" method. Instead, if such mobile electrons or green dots are almost absent at the Fermi level like in Figure 8b, we ought to construct the CG−TH−HR curve or the NFE curve by taking the CG energy as described above. The latter becomes inevitable when the Fermi level enters deeply into the d band and also when a deep true gap (or pseudogap) opens at the Fermi level.

4. RESULTS AND DISCUSSION

4.1. van Arkel−Ketelaar Triangle Map beyond the Allen Electronegativity Approach. Allen[31] noted that only diatomic covalent bonds occur in N_2, O_2, and F_2, where χ_{spec} in eq 1 is very high because s and p atomic levels ε_s and ε_p are widely separated. As we move to the left along a given row of the Periodic Table, the energy level spacing decreases and χ_{spec} decreases accordingly. This is the basic idea behind the Allen electronegativity concept. We consider it to be worthwhile to rewrite eq 2 by using FLAPW-derived parameters, which can easily be calculated for elements as well as for equiatomic compounds.

A change in the contribution of covalency relative to metallicity from one element to another across a given period

dx.doi.org/10.1021/ic502286q | Inorg. Chem. 2015, 54, 930−946

of the Periodic Table may be better judged from a difference in the CG energies of FLAPW-derived s and p partial DOSs in an element:

$$E_{sp}^{A} \equiv |E_{cg-s}^{A} - E_{cg-p}^{A}| \quad (7)$$

where E_{cg-s}^{A} and E_{cg-p}^{A} represent the CG energy of s and p partial DOSs of pure element A.

Figure 2 shows the s, p, d, and f partial DOSs for bcc Na and orthorhombic Cl situated at the extreme left and right. respectively, in period 3 of the Periodic Table. Both s and p partial DOSs almost fully overlap in Na, taking this as evidence for a typical metallic bond. Instead, the s partial DOS is almost perfectly separated from the p partial one in Cl. The DOS characterized by a series of δ-function-like peaks is typical of covalently bonded solids with directional bonds. As indicated in Figure 2, the FLAPW separation energy E_{sp}^{Na} is only 0.48 eV, while E_{sp}^{Cl} is increased to 11.35 eV.

The group number dependence of E_{sp}^{A} for elements in periods 3 and 4 is shown in Figure 3a in comparison with that of Allen's electronegativity χ_{spec} in Figure 3b. The overall behavior is quite similar for the two, and the data for elements in both periods 3 and 4 fall on a master curve. It is emphasized that the FLAPW separation energy E_{sp}^{A} remains more or less constant at about 2 eV for TM 3d elements except for the early ones such as Sc and Ti. A careful inspection of changes in the valence band structure with increasing atomic number reveals that the DOS below the Fermi level forms a continuous free-electron-like band from Na up to Al but tends to be separated into s and p components while still maintaining a continuous band in Si and P. However, it is split into many peaks separated by energy gaps in S and Cl. This is indeed taken as a reflection of the gradual shift from metallicity to covalency across the Periodic Table. As is clear from the argument above, the FLAPW E_{sp}^{A} could serve as a covalency indicator in the substitution of χ_{spec} employed by Allen.

The covalency indicator given by eq 7 for pure element A may be naturally extended to an equiatomic binary compound AB in the following form:

$$E_{sp}^{AB} \equiv (|E_{cg-s}^{A\text{ in }AB} - E_{cg-p}^{A\text{ in }AB}| + |E_{cg-s}^{B\text{ in }AB} - E_{cg-p}^{B\text{ in }AB}|)/2 \quad (8)$$

where $E_{cg-s}^{A\text{ in }AB}$ represents the CG energy of the FLAPW-derived s partial DOS of constituent element A in equiatomic compound AB. Equation 8 may be more rigorously used for equiatomic compounds.

Both E_{sp}^{A} and E_{sp}^{AB} data calculated from eqs 7 and 8 must be transferred into an explicit position in the triangle through the relationship $X = \alpha E_{sp}^{AB} + \beta$, where X is a variable to specify the degree of covalency. The coefficients α and β were determined to be 9.20 and 4.42 from the constraints $(X, E_{sp}^{Na}) = (0, 0.48)$ at the vertex M and $(X, E_{sp}^{Cl}) = (100, 11.35)$ at the vertex C (see Figure 2). The values of X for 26 equiatomic compounds that we studied were distributed over the range from 10 for AlMn to 49 for NaCl. The value of $X = 49$ for NaCl must be replaced by $X = 0$ to force it to be positioned at the vertex I.

Let us now discuss whether $\Delta\chi_{AB}$ given by eq 3 can also be replaced by a quantity derived from FLAPW band calculations. As emphasized above, metallic and covalent bonds must be equally treated in quantum mechanics because the degree of extension of electron wave functions across a crystal determines the respective contributions. This has certainly driven us to rely on eqs 7 and 8 instead of eq 2 inherent to free atoms. In contrast, we are aware that the cohesive energy in an ideally ionic crystal can be calculated by summing up an electrostatic Madelung energy for an assembly of ions with unlike charges within the framework of classical electrodynamics. In this sense, the Allen electronegativity may be more favorable in the evaluation of ionicity because it is free from band-structure effects such as local atomic arrangements, crystal structure, and unit cell size.

Three possible quantities were tested as an ionic indicator: (I) Allen's definition given by eq 3, (II) a difference in the CG energies between the s and p states of pure elements A and B, and (III) a difference in the CG energies between the s and p states of the constituent elements A and B in an AB compound. In case II, for example, the degree of ionicity for an AB compound is given by a difference in eq 7 between the elements A and B, i.e., $|E_{sp}^{A} - E_{sp}^{B}|$:

$$\Delta E_{sp}^{AB} \equiv |E_{sp}^{A} - E_{sp}^{B}| = ||E_{cg-s}^{A} - E_{cg-p}^{A}| - |E_{cg-s}^{B} - E_{cg-p}^{B}|| \quad (9)$$

where E_{cg-s}^{A} and E_{cg-p}^{A} represent the CG energies of s and p partial DOSs calculated for pure element A. The ionicity indicator ΔE_{sp}^{AB} calculated from eq 9 can be transferred into the triangle through the relationship $Y = \gamma \Delta E_{sp}^{AB}$ (%). The coefficient γ is determined to be 9.2 by imposing the constraint $(Y, \Delta E_{sp}^{AB}) = (100, 10.87)$ on NaCl (see Figure 2). The variable Y is distributed from zero for AlMn to 100 for NaCl. The transfer of the data to the triangle can be similarly made for case III.

The three different van Arkel−Ketelaar triangles were constructed in this way by using E_{sp}^{AB} in eq 8 for covalency and cases I−III for ionicity for the 26 equiatomic compounds (eq 7 is employed for pure elements). The data points are most sharply distributed in case I. Instead, its distribution is smeared and randomized, as we go from case I to II and further to case III. Case III involves all kinds of band-structure effects including those caused by interactions between constituent atoms A and B in the compound. The band-structure effects in case II are weakened relative to those in case III because alloying effects between the atoms A and B are absent. In contrast, case I based on the Allen electronegativity difference is completely free from any band-structure effects.

Figure 4 is constructed by employing eq 8 to assess the covalency and Allen's electronegativity difference given by eq 3 to assess the ionicity for the 26 equiatomic compounds. In the same manner as that in Figure 1, the electronegativity difference is transferred to the triangle through $Y = c\Delta\chi_{AB}$ with $c = 50$ for NaCl and $c = 40$ for the rest. It is clear from Figure 4 that the first two elements, Mg and Al, are situated at 8 and 12%, respectively, near the vertex M, while the last two elements, P and S, are at 50 and 70%, respectively, on the side MC and widely separated from each other. This is in sharp contrast to the more or less even distributions of these elements in Figure 1, where Mg, Al, P, and S are found at 20, 37, 70, and 87%, respectively, on the side MC. This unique difference obviously stems from a sharp difference between parts a and b of Figure 3, where the FLAPW E_{sp} data are distributed over a wide range from 0 to 12 and the last five elements, Al, Si, P, S, and Cl, fall on a line with a slope much steeper than the first three elements, Na, Mg, and Al, do, while the Allen electronegativity data are more or less evenly distributed over a narrower range from 0 to 3.

We believe that a fresh insight has been gained into the physics behind the van Arkel−Ketelaar triangle by carrying out FLAPW-based analysis. More important to be noted is the

dx.doi.org/10.1021/ic502286q | Inorg. Chem. 2015, 54, 930−946

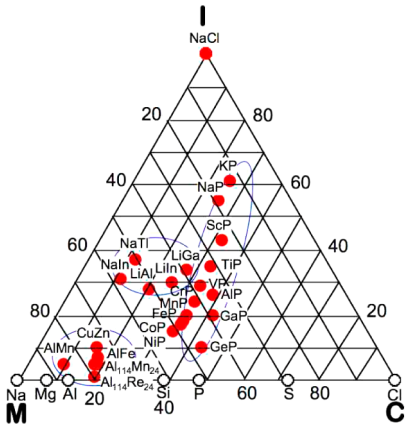

Figure 4. van Arkel−Ketelaar triangle constructed by inserting the Allen electronegativity data[30,31] into eq 3 for ionicity and the FLAPW separation energies into eq 7 for seven elements in period 3 (○) and into eq 8 for the equiatomic binary compounds (red solid circle). Equiatomic Zintl compounds AX (A = Li and Na and X = Al, Ga, In, and Tl), Al−TM compounds, and P-based compounds are circled in blue to distinguish one from another.

finding that the data for a series of P-based compounds commonly fall on an almost vertical narrow strip and are clearly separated from a series of Zintl and Al−TM compounds, as can be seen in both Figures 1 and 4. In the rest of our discussions, we will use Figure 1 more frequently as a guide. In particular, one has to rely on Figure 1 when an equiatomic compound is not available in the literature.[34]

Let us now discuss how the ionicity changes as a result of the systematic selection of the partner element in P-based intermetallic compounds. The ionicity reaches a maximum of 64% in CsP and is distributed over the range 53−64% in AP (A = Li, Na, K, Rb, and Cs) compounds, where alkali metal A in group 1 is located farthest from P. Next to A−P compounds, CaP, a combination of a divalent element with P, is positioned at about 50% ionicity. Among the equiatomic TM−P compounds, ScP possesses the largest ionicity of 43%. The value gradually decreases with increasing atomic number up to NiP. The ionicity in GaP and AlP is at about 25%. The GeP compound obtained by selecting the partner element Ge from group 14 is characterized by a relatively low ionicity of 10% and is the lowest among the P compounds studied. It is interesting to note that the metallicity and covalency are in the ranges 5−30% and 30−65%, respectively, in all selected P-based intermetallic compounds.

It is also worth mentioning that a series of Zintl compounds (cF32) are positioned in the ranges of 28−38% ionicity, 40−55% metallicity, and 20−25% covalency. This is consistent with the possession of a rather free-electron-like DOS, as revealed in FLAPW−Fourier analysis.[26] It is also noted that the Al−TM compounds are positioned in an area with a fairly small ionicity of less than 10% and a covalency of 40% between the free-electron-like Al and more covalently bonded Si elements. The area where Al−TM compounds fall is shifted to the left in Figure 4, although it is still found between Al and Si. We consider this to be consistent with the presence of strong orbital hybridization effects in MI-type quasicrystals and their approximants, which are responsible for the formation of a pseudogap across the Fermi level. In the following sections, we will make full use of the van-Arkel−Ketelaar triangles shown in Figures 1 and 4 and discuss whether the Fermi surface−Brillouin zone interactions can be extracted and the value of e/a can be safely determined as the ionicity is increased in P-based intermetallic compounds.

4.2. e/a Determination of P-Based Compounds. *4.2.1. e/a for Pure Elements P, As, Sb, and Bi in Group 15.* To begin with, we show the partial DOS and the Hume-Rothery plot for the parent element P in parts a and b of Figure 5, respectively. Although its valence band is still continuous, it is divided into many sharp peaks with a deep pseudogap across the Fermi level. This is due to the growth of directional bonding characteristic of covalent bonds in P. This is in sharp contrast to the free-electron-like valence band structure of Na, on the one hand, and Cl, on the other hand, as shown in Figure 2. The FLAPW separation energy E_{sp}^{P} = 5.74 eV lies in the middle of the two extremes, E_{sp}^{Na} = 0.48 eV for Na and E_{sp}^{Cl} = 11.35 eV for Cl, thereby resulting in its location at about 70% covalency on the MC line in Figure 1.

As shown in Figure 5b, the TH−HR data points (black curve) almost fall on a straight line with small up and down anomalies obviously due to spiky DOS peaks in part a. The CG−TH−HR or NFE curve (red line), described in section 3.3, is almost linear over the entire energy range because small anomalies in the TH−HR data are well suppressed. Note that the local reading method is, in principle, validated for P, but the NFE curve is used to get rid of small anomalies across the Fermi level. The value of the square of the Fermi diameter, $(2k_F)^2$, is determined to be 11.52 in units of $(2\pi/a)^2$ by reading

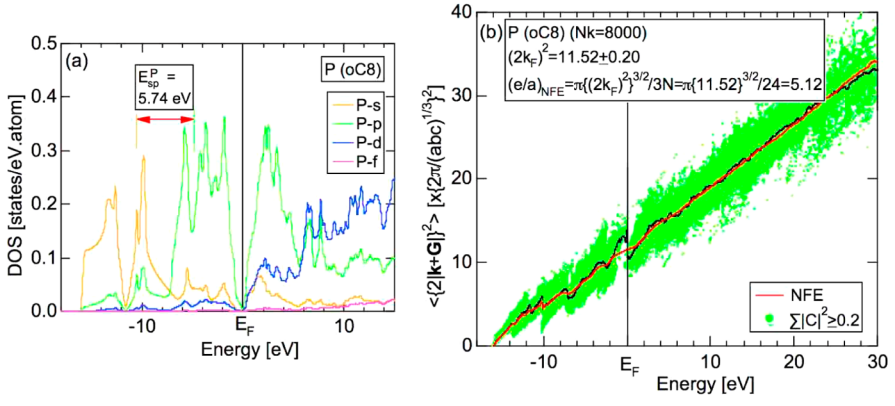

Figure 5. Computed data for the orthorhombic P (oC8) compound: (a) P partial DOSs and its separation energy E_{sp}^{P}; (b) the Hume-Rothery plot. The TH−HR data points (black), NFE curve (red), and (neon green solid circle) data points satisfying the condition $\sum|C^{j}_{k_i+G_p}|^2 \geq 0.2$.

dx.doi.org/10.1021/ic502286q | Inorg. Chem. 2015, 54, 930−946

Table 1. Electronic Parameters of Group 15 Elements of the Periodic Table

system	space group	Pearson symbol	$\|G\|_c^2[(2\pi/a)^2]$	$(2k_F)^2[(2\pi/a)^2]$	e/a
P	*Cmca*	oC8	10.56	11.52	5.12 ± 0.10
As	$R\bar{3}m$	hR2	4.74	4.45	4.92 ± 0.14
Sb	$R\bar{3}m$	hR2	4.54	4.50	5.00 ± 0.15
Bi	$R\bar{3}m$	hR2	4.53	4.48	4.97 ± 0.25

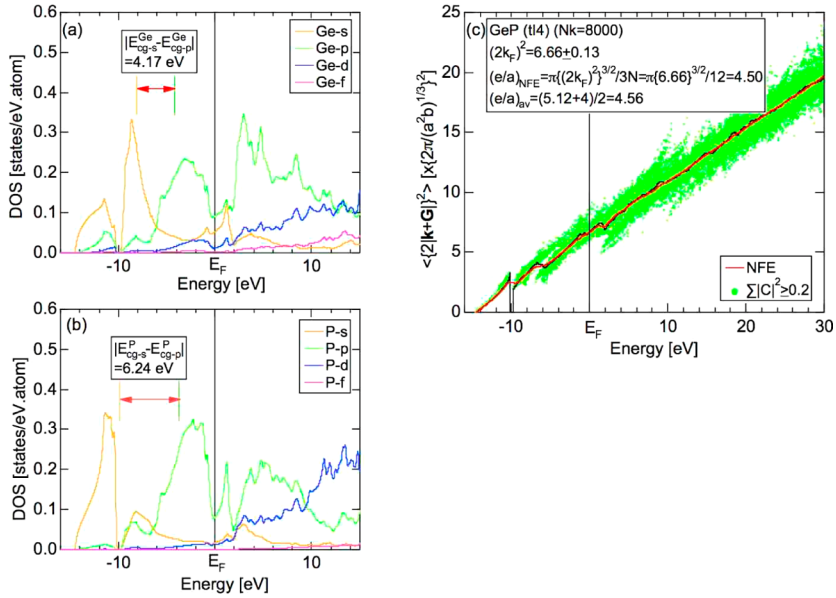

Figure 6. Computed data for the GeP (tI4) compound: (a) Ge partial DOSs and its separation energy E^{Ge}_{sp}; (b) P partial DOSs and its separation energy E^{P}_{sp}; (c) the Hume-Rothery plot. For the meaning of the symbols, see Figure 5.

off the ordinate at the Fermi level. The value of e/a is calculated to be 5.12 by inserting $(2k_F)^2$ thus obtained into the well-known relationship:

$$e/a = \frac{\pi\{(2k_F)^2\}^{3/2}}{3N} \tag{10}$$

where N is the number of atoms in the unit cell. This is consistent with the possession of its nominal valency of 5. This demonstrates that the value of e/a can be well-determined in spite of its location in the middle of the side MC in Figures 1 and 4. Similarly, the e/a values of As, Sb, and Bi in group 15 of the Periodic Table were also found to be very close to 5, as listed in Table 1, into which relevant electronic parameters are also incorporated.

4.2.2. AlP, SiP, GaP, and GeP Intermetallic Compounds. According to the phase diagram of the M−P (M = Al, Ga, Si, and Ge) alloy systems,[35] a stable phase is formed only at the equiatomic composition. Both AlP and GaP crystallize into a cubic phase with space group $F\bar{4}3m$ and Pearson symbol cF8, while GeP crystallizes into a tetragonal phase with space group $I4mm$ and Pearson symbol tI4 and SiP into an orthorhombic phase with space group $Cmc2_1$ and Pearson symbol oC48. As can be seen from Figure 4, they are characterized by a covalency of 60% and an ionicity of about 10−25%.

As is representative in this family, both the Ge and P partial DOSs in GeP are shown in Figure 6a,b. The FLAPW separation energy E^{GeP}_{sp} is deduced to be 5.21 eV from eq 8. This is slightly smaller than E^{P}_{sp} = 5.74 eV for element P. As shown in Figure 6c, the NFE curve (red) passes through the TH−HR data points (black) over the entire energy range. There is no measurable difference, depending on whether the local reading method or the NFE curve is used. The resulting e/a value is in good agreement with the value of 4.56 obtained from composition averages of $(e/a)_{Ge}$ = 4.0 and $(e/a)_{P}$ = 5.12.

4.2.3. TM−P (TM = Sc−Ni) Intermetallic Compounds. Before going into the detailed e/a analysis for TM−P (TM = Sc−Ni) compounds, we briefly review the FLAPW−Fourier analysis previously made on a series of M−Al (M = K−Cu) compounds, as reported by Sato et al.[24] From the M concentration dependence of e/a for M−Al (M = K−Cu) intermetallic compounds, they determined the e/a value of the element M. The e/a values for K and Ca are safely deduced to be 1.0 and 2.0, respectively, by employing the local reading method because electrons at the Fermi level are highly itinerant. These values are in perfect agreement with their nominal valences of unity and 2. The e/a value for Sc, the first TM 3d element, where the Fermi level moves into the early phase of the Sc 3d band, is deduced to be 2.94, in good agreement with the metallic valence of 3 proposed by Pauling.[14] Here again electrons at the Fermi level are judged to be itinerant, thereby allowing us to rely on the local reading method.[23,24]

As we progress further to the right in the Periodic Table, the Fermi level penetrates deeper and deeper into the 3d band. The construction of the CG−TH−HR or the NFE curve becomes mandatory for TM elements from Ti to Co. The effective e/a values for the TM 3d elements from Ti to Co are distributed in the vicinity of unity, in disagreement with the negative e/a values reported by Raynor in 1949.[13] Among them, Ti is marginal. The local reading method without introducing the NFE approximation yields e/a = 3.90, close to the 4 derived by assuming all four outermost electrons including 3d electrons to

dx.doi.org/10.1021/ic502286q | *Inorg. Chem.* 2015, 54, 930−946

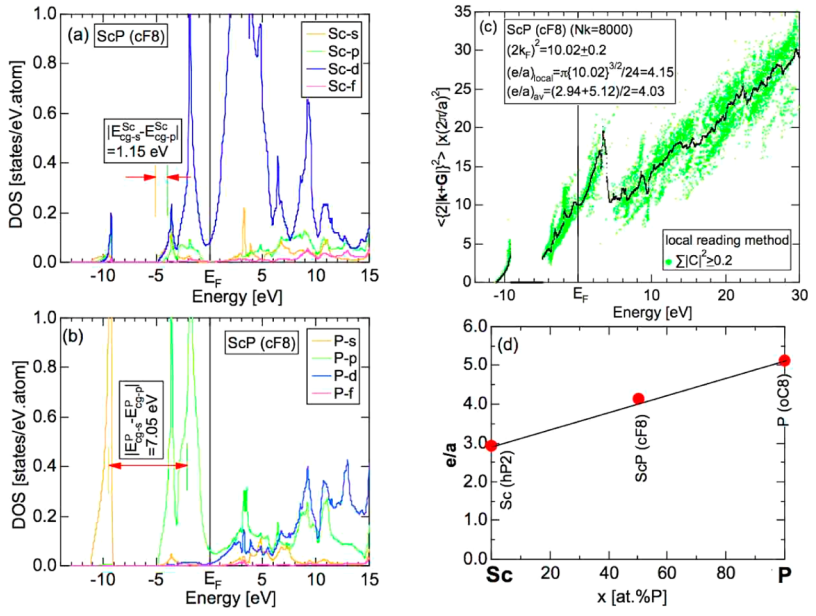

Figure 7. Computed data for the ScP (cF8) compound: (a) Sc partial DOSs and its separation energy E_{sp}^{Sc}; (b) P partial DOSs and its separation energy E_{sp}^{P}; (c) the Hume-Rothery plot; (d) P concentration dependence of e/a subjected to the local reading method in the Sc−P alloy system. For the meaning of the symbols, see Figure 5.

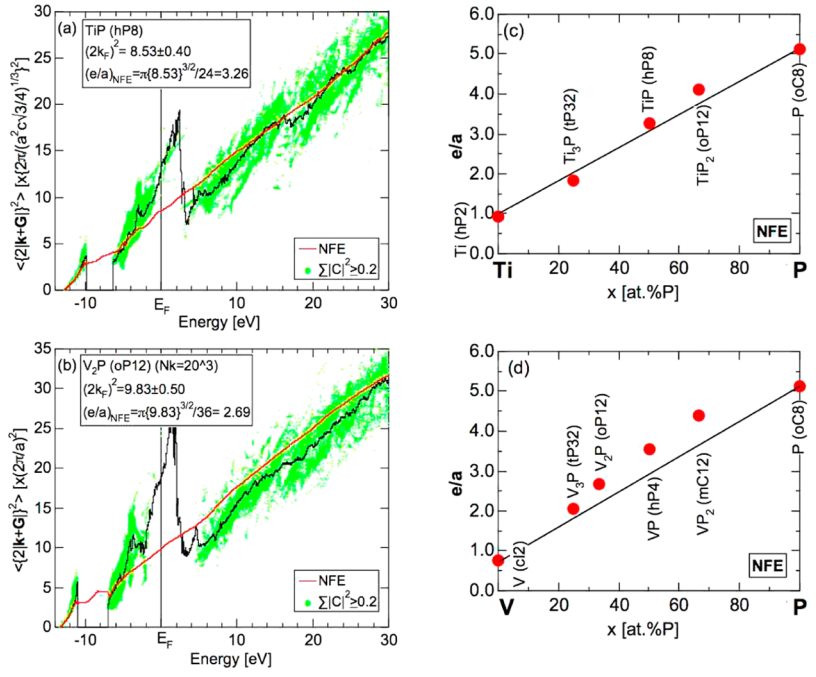

Figure 8. (a) Hume-Rothery plot for the TiP (hP8) compound and (b) that for the V_2P (oP12) compound and (c) P concentration dependence of e/a subjected to the NFE approximation in the Ti−P alloy system and (d) that in the V−P alloy system. For the meaning of the symbols, see Figure 5.

be itinerant. Instead, e/a = 0.92 was derived from the NFE curve.

Keeping in mind the work for TM−Al compounds, we start to determine e/a values for TM−P (TM = Sc−Cu) binary compounds. Only the equiatomic ScP (cF8) compound exists as a stable phase in the Sc−P alloy system. The Sc and P partial DOSs, Hume-Rothery plot, and P concentration dependence of e/a are shown in parts a−d of Figure 7, respectively. The data for Sc itself has already been discussed.[24] The FLAPW separation energy associated with the Sc s and p states is 1.15 eV, while that with the P s and p states is 7.05 eV. Thus, the value of E_{sp}^{ScP} deduced from eq 8 becomes 4.1 eV. The ionicity determined from eq 3 turns out to be $\Delta\chi_{spec}^{ScP} = |\chi_{spec}^{Sc} - \chi_{spec}^{P}| = |1.19 - 2.253| = 1.063$.[32] As shown in Figure 1, ScP is characterized by a high ionicity of 43% and a covalency of 42%.

The value of e/a for ScP is determined from the Hume-Rothery plot shown in Figure 7c. The local reading method can be safely used for ScP because mobile electrons satisfying $\sum|C^{i}_{k_i+G_p}|^2 \geq 0.2$ (green dots) are abundant at the Fermi level. The effective e/a value is determined to be 4.15, in good

dx.doi.org/10.1021/ic502286q | Inorg. Chem. 2015, 54, 930−946

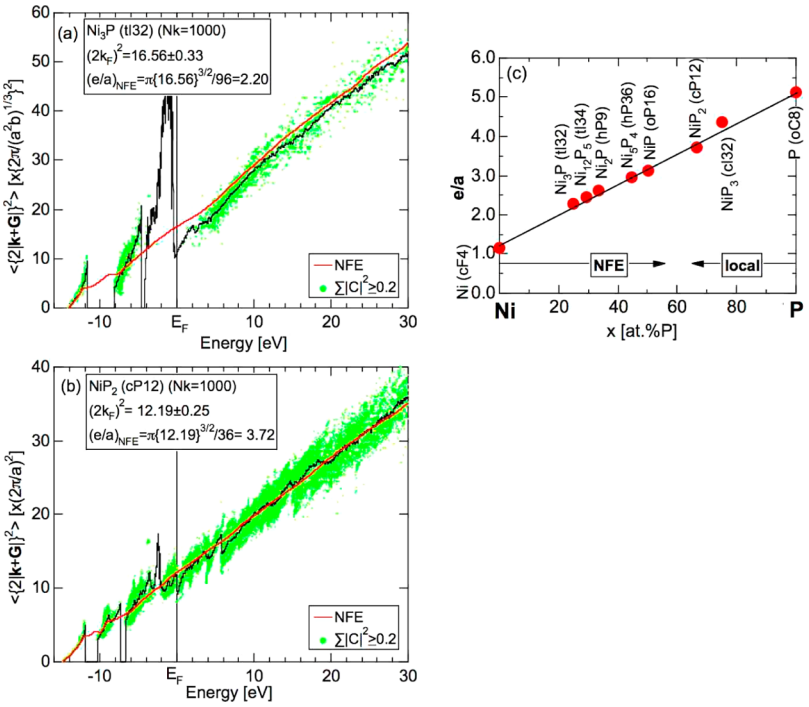

Figure 9. (a) Hume-Rothery plot for the Ni_3P (tI32) compound. (b) Hume-Rothery plot for the NiP_2 (cP12) compound. For the meaning of the symbols, see Figure 5. (c) P concentration dependence of e/a in the Ni−P alloy system. The local reading method can be employed for P-rich compounds, while the NFE curve is constructed for Ni-rich compounds including pure Ni.

agreement with composition average of $(e/a)_{Sc}$ = 2.94 and $(e/a)_P$ = 5.12, as shown in Figure 7d. It is worth noting that an error bar is not indicated because it lies within the diameter of the red circle data point. This means that e/a can be safely determined even for polar compounds with ionicity and covalency exceeding 40%.

There are three and four intermetallic compounds in the Ti−P and V−P alloy systems, respectively.[34] Both TiP and VP compounds are 30−35% in ionicity and are located below the ScP compound in the van Arkel−Ketelaar triangle. As representatives, we show the Hume-Rothery plot for TiP (hP8) and V_2P (oP12) in parts a and b of Figure 8, respectively. The green dots in TiP are not many but still sufficient in number at the Fermi level. Ti and its compounds are indeed marginal in the selection of either the local reading method or NFE approximation. Instead, green dots are absent at the Fermi level in the V_2P compound (see Figure 8b). The P concentration dependence of e/a determined from the NFE curve is shown in parts c and d of Figure 8 for Ti−P and V−P alloy systems, respectively. We learn that the e/a value for both alloy systems can be reproduced within ±10% by taking composition averages of $(e/a)_{Ti}$ = 0.92, $(e/a)_V$ = 0.76, and $(e/a)_P$ = 5.12. The simple linear interpolation method has been confirmed to hold true in many Al−TM alloy systems.[24,25] The present result demonstrates that this simple rule holds true in polar intermetallic compounds with ionicity higher than 30%.

The P concentration dependence of e/a has been similarly determined in the rest of the TM−P (TM = Cr, Mn, Fe, Co, Ni, and Cu) alloy systems: Cr_3P (tP32), $Cr_{12}P_7$ (hP19), CrP (oP8), and CrP_2 (mC12) in the Cr−P alloy system, Mn_3P (tP32), MnP (oP8), and MnP_4 (aP10) in the Mn−P alloy system, Fe_3P (tP32), Fe_2P (hP9), FeP (oP8), FeP_2 (oP6), and FeP_4 (mC40) in the Fe−P alloy system, CoP (oP8), CoP_2 (mP12), and CoP_3 (cI32) in the Co−P alloy system, Ni_3P (tI32), $Ni_{12}P_5$ (tI34), Ni_2P (hP9), Ni_5P_4 (hP36), NiP (oP16), NiP_2 (cP12), and NiP_3 (cI32) in the Ni−P alloy system, and Cu_3P (hP24), CuP_2 (mP12) and Cu_2P_7 (mC72) in the Cu−P alloy system. The use of the NFE approximation is mandatory for TM = Cr, Mn, Fe, and Co because the Fermi level falls deep inside the d band, while the local reading method has to be resumed for P-rich Ni−P compounds, where the Fermi level escapes from the Ni 3d band.[24] Below, we show the recovery of the local reading method for P-rich Ni−P compounds.

As emphasized above, Ti and its compounds are marginal in the choice of either the local reading method or the NFE approximation as the early-TM family. Another marginal situation is encountered in Ni and its compounds as the late-TM family because the addition of polyvalent elements like Al and P raises the Fermi level above the Ni 3d band and drastically changes its electronic structure to that similar to noble metals, where the use of the local reading method is required.[24] In the case of Al-rich Ni compounds, the value of $(e/a)_{Ni}$ was deduced to be zero, while that for pure Ni and Ni-rich compounds was 0.5. It was claimed that the e/a determination for Ni−Al, Pd−Al, and Pt−Al compounds is sensitive to the solute concentration.[24,25]

The Hume-Rothery plot for Ni_3P (tI32) is shown in Figure 9a, in comparison with that for NiP_2 (cP12) in Figure 9b. One can immediately notice that, in the case of Ni_3P, the slope of a line passing through TH−HR data points and green dots in the energy region over −8 to −4 eV is entirely different from those in the energy region above +4 eV and that green dots are absent at the Fermi level. This requires us to rely on the NFE approximation to determine its e/a value. In contrast, green dots are almost uniformly distributed on a single line over a whole energy region through the Fermi level in P-rich NiP_2, as shown in Figure 9b. This essentially validates the choice of the local reading method. However, to smooth out anomalies, we

dx.doi.org/10.1021/ic502286q | Inorg. Chem. 2015, 54, 930−946

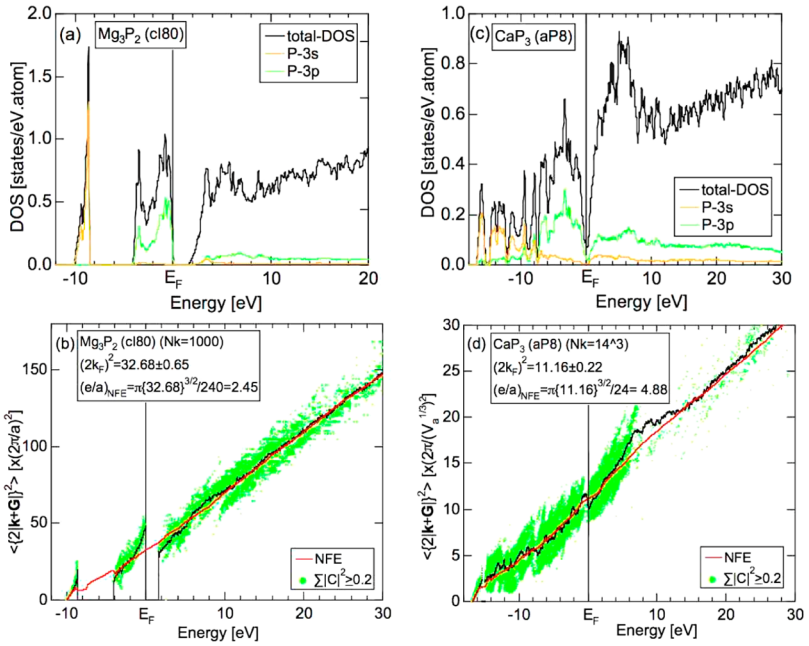

Figure 10. Computed data for the Mg_3P_2 (cI80) compound: (a) total and P 3s and 3p partial DOSs; (b) the Hume-Rothery plot. For the meaning of the symbols, see Figure 5. Computed data for the CaP_3 (aP8) compound: (c) total and P 3s and 3p partial DOSs; (d) the Hume-Rothery plot. For the meaning of the symbols, see Figure 5.

constructed the NFE curve. The same treatment was applied to NiP_3 (cI32) and pure P (oC8) shown in Figure 5b. The P concentration dependence of e/a is shown in Figure 9c. As emphasized above, one needs to employ the NFE approximation below 50 atom % P but can essentially resume the local reading method for P-rich compounds. [The local reading method was employed for pure Ni (cF4) and yielded $(e/a)_{Ni}$ = 0.50.[24] In the present studies, however, we judged the NFE approximation to be used rather than the local reading method for Ni-rich compounds including pure Ni. The NFE curve with L higher than 10 was needed in the case of pure Ni to completely suppress the Ni 3d band anomaly at the Fermi level. The e/a = 1.16 thus obtained for Ni is plotted in Figure 9c.]

In summary, the e/a values are found to fall on a straight line connecting e/a values of the parent elements, regardless of whether the local reading or NFE method was employed for TM−P compounds: $(e/a)_{Sc}$ = 2.94, $(e/a)_{Ti}$ = 0.92, $(e/a)_{V}$ = 0.76, $(e/a)_{Cr}$ = 0.92, $(e/a)_{Mn}$ = 1.05, $(e/a)_{Fe}$ = 1.05, $(e/a)_{Co}$ = 1.11, $(e/a)_{Ni}$ = 1.16, $(e/a)_{Cu}$ = 1.00, and $(e/a)_{P}$ = 5.12. The linear interpolation method is confirmed to hold true in TM−P alloy systems covering an ionicity up to 43% in ScP.

4.2.4. Mg−P, Ca−P, and Zn−P Intermetallic Compounds. According to *Pearson's Handbook*,[34] structural information is available for several intermetallic compounds in Mg−P, Ca−P, and Zn−P alloy systems: Mg_3P_2 (cI80) and MgP_4 (mP10), Ca_5P_8 (mC26) and CaP_3 (aP8), and Zn_3P_2 (tP40), ZnP_2 (mP24), and ZnP_4 (tP20). Because there are no equiatomic compounds, the FLAPW separation energy cannot be evaluated. Thus, Allen's electronegativity table[32] is used for hypothetical MgP, CaP, and ZnP compounds to fill their data in Figure 1. As shown in Figure 1, the ionicity of CaP is 49% and higher than that of ScP already discussed. Instead, the ionicity of MgP and ZnP is in the range 30−40% and similar to those of TiP, VP, and AlP.

As representatives, we show in parts a and b of Figure 10 the DOS and Hume-Rothery plot for Mg_3P_2 (cI80) in comparison with those for CaP_3 (aP8) in parts c and d of Figure 10, respectively. The DOS below the Fermi level in Mg_3P_2 is split into two components mainly made up of P 3s and 3p states. This is also true in TiP and V_2P discussed above. It is interesting to note that the ionicity in these three compounds is commonly found in the range 30−40%. Instead, the DOS splits into many peaks below the Fermi level in CaP_3, indicating the growth of directional bondings (see Figure 10c). This is obviously caused by an increase in the ionicity up to 50%. The characteristic features in the DOS are well-reflected in the Hume-Rothery plots in Figure 10d. A fairly smooth NFE curve is constructed to suppress anomalies caused by a deep pseudogap at the Fermi level and many spiky DOS peaks in CaP_3. The situation in Zn−P compounds was found to be intermediate between Mg−P and Ca−P compounds. The values of $(2k_F)^2$ and e/a are determined from the intersection of its NFE curve with the Fermi level. The resulting e/a values were found to fall on the linear interpolation lines connecting $(e/a)_{Ca}$ = 2.00, $(e/a)_{Mg}$ = 2.00, $(e/a)_{Zn}$ = 2.04, and $(e/a)_{P}$ = 5.12.

In summary, the ionicity is around 30, 40, and 50% in the Zn−P, Mg−P, and Ca−P compounds, respectively. The higher the ionicity, the more frequently the valence band tends to split into spiky peaks and thereby the more anomalies appear in the TH−HR curve. Nevertheless, we can say that both $(2k_F)^2$ and e/a values are still safely and consistently determined from the NFE curve for polar compounds with ionicity of less than 50%.

4.2.5. A−P (A = Li, Na, K, Rb, and Cs) Intermetallic Compounds. Among the alkali metal−phosphorus (A−P) binary alloy systems, an equiatomic compound apparently exists only in the Na−P and K−P alloy systems.[34] Their data are incorporated into Figure 4. In addition, the data on hypothetical equiatomic compounds LiP, RbP, and CsP are added to Figure 1 by using the Allen electronegativity table.[32] We have studied all intermetallic compounds available from ref 34 in the A−P (A = Li, Na, K, Rb, and Cs) alloy systems: Li_3P

dx.doi.org/10.1021/ic502286q | *Inorg. Chem.* 2015, 54, 930−946

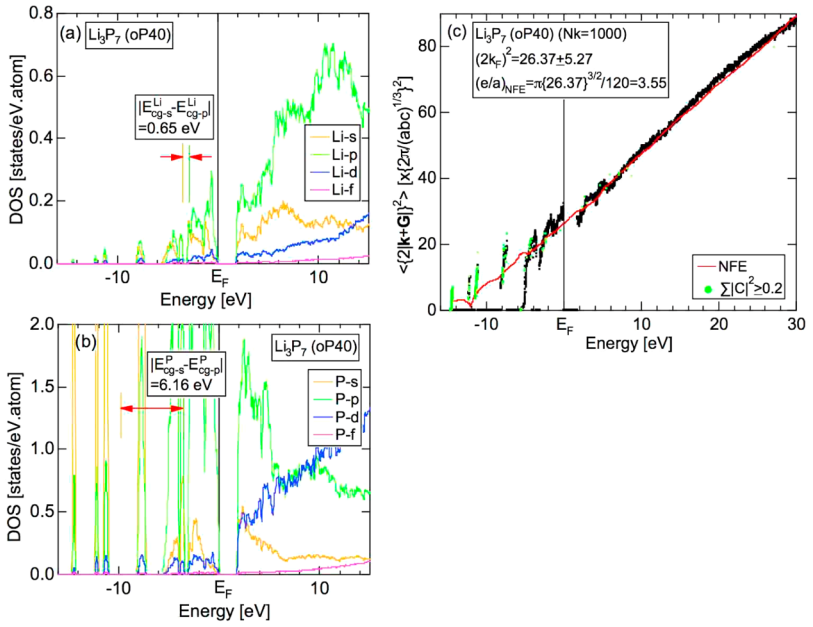

Figure 11. Computed data for the Li_3P_7 (oP40) compound: (a) Li partial DOSs and its separation energy E^{Li}_{sp}; (b) P partial DOSs and its separation energy E^{P}_{sp}; (c) the Hume-Rothery plot. For the meaning of the symbols, see Figure 5.

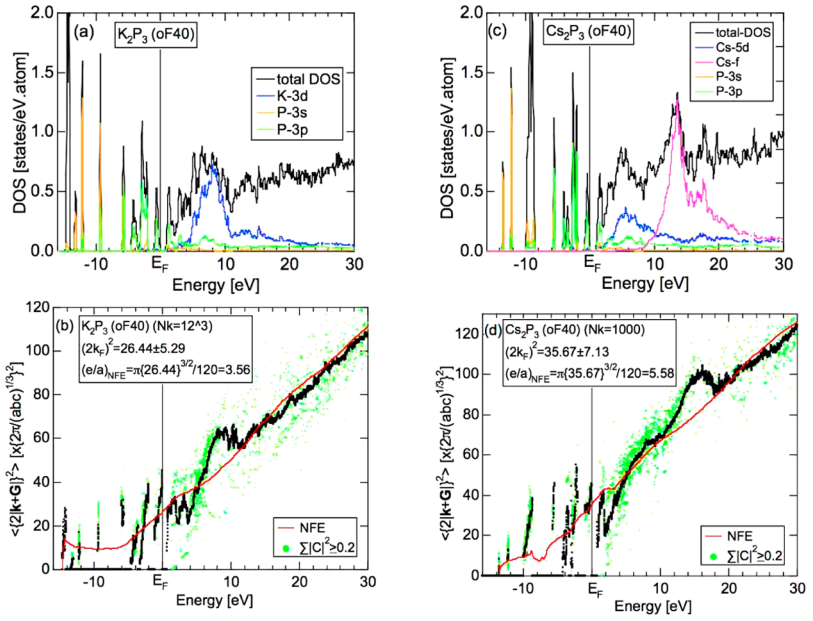

Figure 12. Computed data for the K_2P_3 (oF40) compound: (a) K and P partial DOSs; (b) the Hume-Rothery plot. For the meaning of the symbols, see Figure 5. Computed data for the Cs_2P_3 (oF40) compound: (c) Cs and P partial DOSs; (d) the Hume-Rothery plot. For the meaning of the symbols, see Figure 5.

(hP8), Li_3P_7 (oP40), and LiP_5 (oP24), Na_3P (hP8), NaP (oP16), and Na_3P_{11} (oP56), K_3P (hP8), KP (oP16), K_2P_3 (oF40), and K_3P_{11} (oP56), Rb_2P_3 (oF40), and Cs_2P_3 (oF40) and Cs_3P_7 (tP40).

Parts a–c of Figure 11 show the Li and P partial DOSs and Hume-Rothery plot for the Li_3P_7 (oP40) compound, respectively. The ionicity of LiP is about 53% and is higher than that of CaP discussed above. As can be seen from Figure 11b, the P partial DOS splits into many isolated peaks below the Fermi level, indicating the growth of strong directional bonds as a result of an increase in the ionicity. The separation energy in the Li partial DOS is only 0.65 eV, while that in the P partial DOS is 6.16 eV.

The TH–HR data points in Figure 11c are discontinuous owing to repeated openings of energy gaps below the Fermi level. Thus, the CG–TH–HR or NFE curve has to be constructed. The resulting NFE curve is fairly linear in spite of the frequently disrupted TH–HR data points below the Fermi level. The e/a value turned out to be 3.55, in a reasonable agreement with 3.8 obtained from composition averages of $(e/a)_{Li} = 1.02$ and $(e/a)_P = 5.12$.

As another example, we show in parts a and b of Figure12 the total and K 3d, P 3s, and P 3p DOSs and the Hume-Rothery plot for the K_2P_3 (oF40) compound, respectively. Note that the ionicity of KP reaches 60% and is even higher than that of LiP and NaP. The δ-function-like DOS below the Fermi level is

dx.doi.org/10.1021/ic502286q | Inorg. Chem. 2015, 54, 930–946

apparently sharper than that of Li_3P_7 shown in Figure 11a. Accordingly, the TH−HR data points existing only in limited energy ranges are more widely separated from each other by energy gaps in the valence band, making it more difficult to accurately determine the values of $(2k_F)^2$ and e/a. This is also true in the data for Cs_2P_3 shown in Figure 12c,d. In spite of belonging to isostructural compounds, the e/a value for Cs_2P_3 is much higher than that for K_2P_3. The emergence of Cs 4f states at about 10 eV above the Fermi level may contribute to the enhancement of e/a.

The P concentration dependence of e/a calculated from the NFE curve for all compounds in the A−P (A = Li, Na, K, Rb, and Cs) alloy systems is summarized in Figure 13a−e. One can

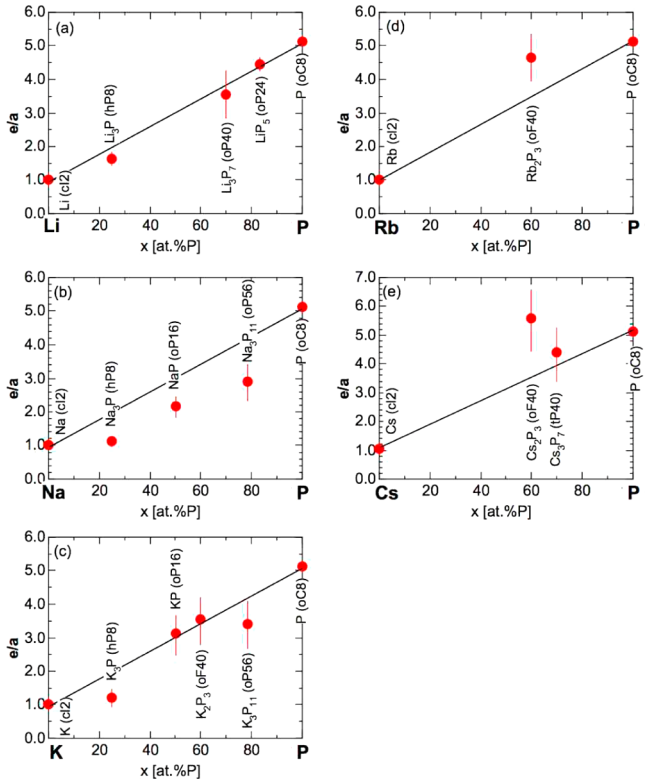

Figure 13. P concentration dependence of e/a subjected to the NFE method for (a) Li−P, (b) Na−P, (c) K−P, (d) Rb−P, and (e) Cs−P alloy systems.

clearly see that an error bar for several compounds reaches 20% of the e/a value determined. This means that the value of e/a has changed by up to 20%, when *WIEN2k* parameters like the number of cells in the Brillouin zone, N_k, and ε_{max} of the energy window are intentionally varied. [In compounds with ionicity of less than 50%, the change in e/a is within 1 to, at most, 5%, being well hidden behind the diameter of the data points (red circle).] This indicates that the e/a determination becomes unstable when the ionicity exceeds 50%. The validity of the linear interpolation rule with $(e/a)_{Li} = 1.02$, $(e/a)_{Na} = 1.00$, $(e/a)_K = 1.00$, $(e/a)_{Rb} = 1.05$, $(e/a)_{Cs} = 1.05$, and $(e/a)_P = 5.12$ in the A−P alloy systems is less satisfactory. Indeed, a significant departure from the line is found to occur in some particular compounds like K_3P_{11} and Cs_2P_3. We learned that, when the ionicity is increased above 50%, the TH−HR data points tend to be more sharply confined in narrow energy ranges and more widely separated from each other by energy gaps in the valence band. Moreover, K 3p, Rb 4p, and Cs 5p core levels begin to merge into the valence band, making it more difficult to specify the bottom of the valence band. All of them are apparently responsible for causing instability in the determination of e/a. The confirmation of the validity of the Hume-Rothery stabilization mechanism and e/a determination as well must be done with great care in polar compounds, where its ionicity is increased above 50%.

4.3. Hume-Rothery Electron Concentration Rule in P-Based Compounds. A strategy in theoretically discovering a new Hume-Rothery electron concentration rule is to find first a group of pseudogap-bearing compounds falling into the same space group and Pearson symbol.[26] This assures the possession of a common set of Brillouin zone planes in reciprocal space. Then a FLAPW−Fourier spectrum is constructed for each of them, which enables us to extract the square of the *critical* reciprocal lattice vector $|\mathbf{G}|_c^2$. Among the isostructural compounds thus studied, we classify them into subgroups with respect to $|\mathbf{G}|_c^2$ thus deduced. This means that compounds in each subgroup should possess the common $(2k_F)^2$, i.e., e/a, because a pseudogap at the Fermi level ensures fulfillment of the interference condition $(2k_F)^2 = |\mathbf{G}|_c^2$.

4.3.1. TMP_3 (TM = Co, Ni, Rh, and Ir), $TMAs_3$ (TM = Co, Rh, and Ir), and $TMSb_3$ (TM = Co, Rh, and Ir; cI32) Skutterudite Compounds. We have recently reported on the theoretical finding of a new Hume-Rothery electron concentration rule in the family of skutterudite compounds.[26] The two partial DOSs, Hume-Rothery plot, and FLAPW−Fourier spectrum for CoP_3 (cI32) are shown in parts a−d of Figure 14, respectively. CoP_3 is known as a typical skutterudite compound and has extensively been studied as a potential thermoelectric material. The FLAPW separation energies associated with Co and P sp

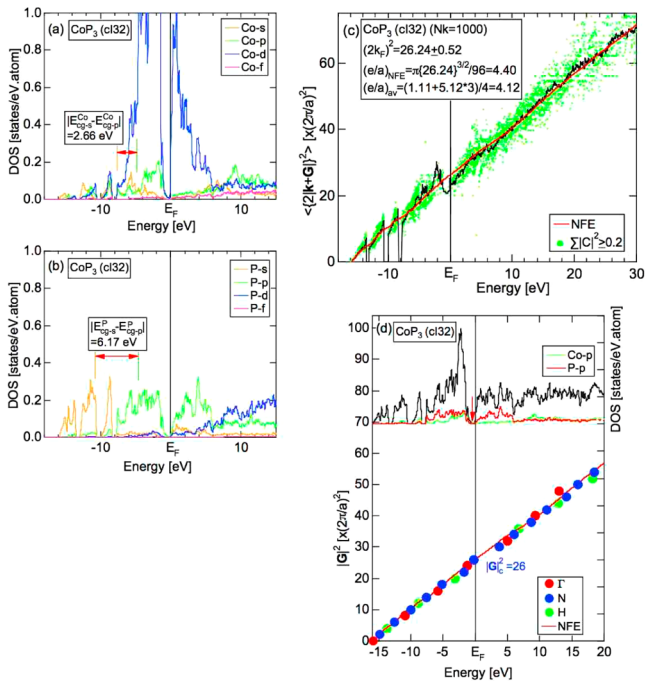

Figure 14. Computed data for the CoP_3 (cI32) compound: (a) Co partial DOSs and its separation energy E_{sp}^{Co}; (b) P partial DOSs and its separation energy E_{sp}^{P}; (c) the Hume-Rothery plot. For the meaning of the symbols, see Figure 5. (d) FLAPW−Fourier spectra at symmetry points Γ, N, and H of the bcc Brillouin zone along with total and Co 4p and P 3p partial DOSs. The NFE curve is duplicated from part c. A red arrow indicates a minimum in the partial DOSs.

dx.doi.org/10.1021/ic502286q | Inorg. Chem. 2015, 54, 930−946

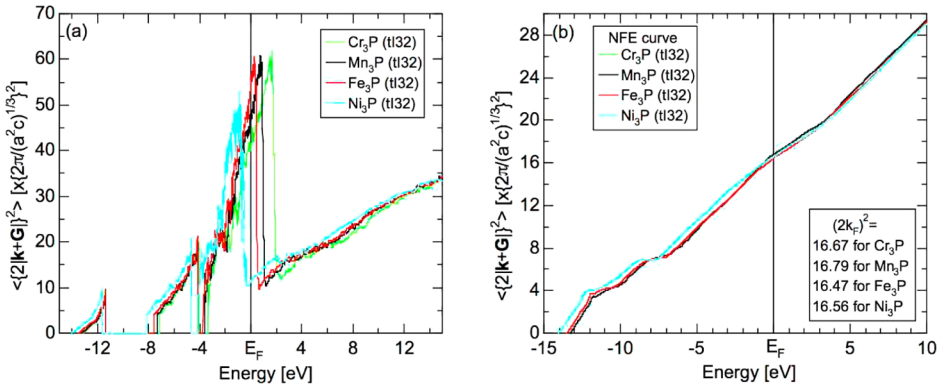

Figure 15. (a) TH−HR data in the Hume-Rothery plot and (b) the NFE curves for TM_3P (TM = Cr, Mn, Fe, and Ni; tI32) compounds. The value of $(2k_F)^2$ in units of $(2\pi/a)^2$ is listed.

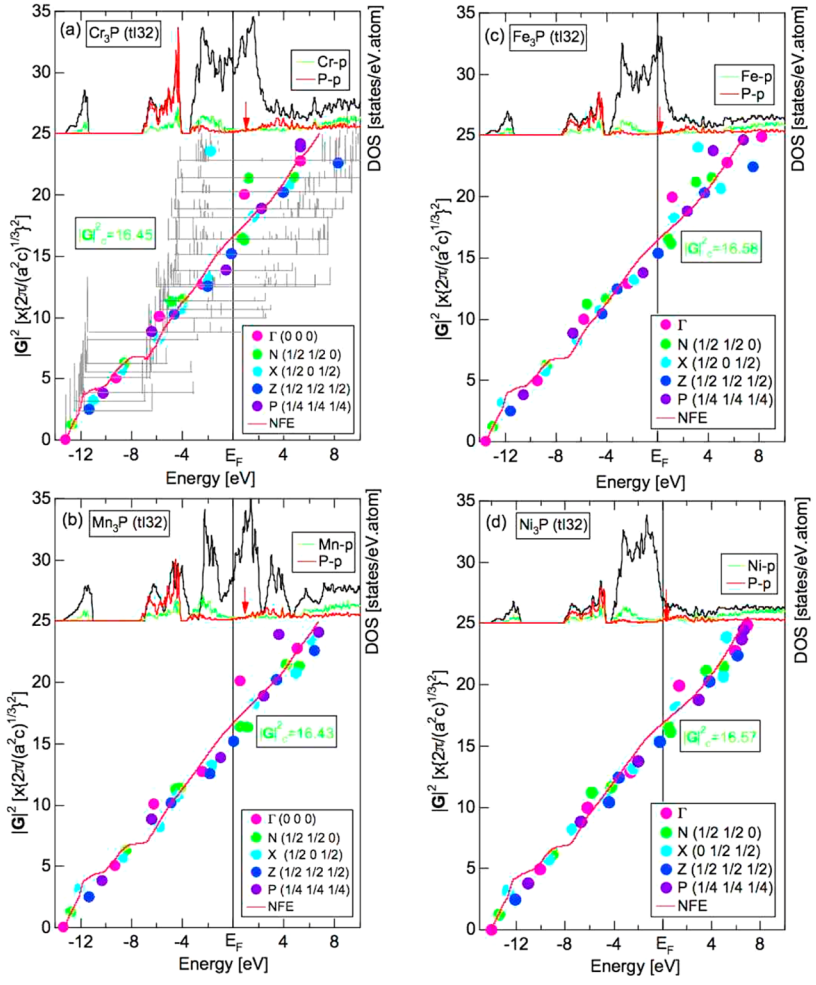

Figure 16. FLAPW−Fourier spectra at symmetry points Γ, N, X, Z, and P in the bct Brillouin zone for (a) Cr_3P, (b) Mn_3P, (c) Fe_3P, and (d) Ni_3P (tI32) compounds along with the respective total (black) and TM 4p (green) and P 3p (red) partial DOSs. A red arrow indicates the minimum in the partial DOSs. The energy dependence of the square of the Fourier coefficients, $\sum|C_G|^2$, is plotted only for Cr_3P in gray. Its CG energy is plotted in parts a−d. The value of $|\mathbf{G}|^2$ obtained from its intersection with the Fermi level is shown as *critical* $|\mathbf{G}|_c^2$.

states turned out to be 2.66 and 6.17 eV, which is slightly different from 2.18 and 6.31 eV, respectively, for the equiatomic compound CoP (oP8) employed in the construction of Figure 4. This certainly reflects a difference in the electronic structure between the two compounds subjected to different alloying environments such as the crystal structure and solute concentration. However, we consider CoP_3 (cI32) to be located near CoP (oP8) in Figure 4 with about 15% ionicity.

The Hume-Rothery plot shown in Figure 14c reveals a series of anomalies below the Fermi level due to opening of energy gaps and a pseudogap at the Fermi level. Moreover, green dots satisfying the condition $\sum|C|^2 \geq 0.2$ and representing itinerant electrons are very scarce at the Fermi level. Thus, we made the

dx.doi.org/10.1021/ic502286q | Inorg. Chem. 2015, 54, 930−946

NFE approximation, as described in section 3.3. The NFE curve is drawn with red in Figure 14c. From its intersection with the Fermi level, we obtain $(2k_F)^2 = 26.24$ and e/a = 4.40, the latter of which is in reasonable agreement with 4.11 obtained from composition averages of $(e/a)_{Co} = 1.11$[24] and $(e/a)_P = 5.12$ (see Figure 5).

The CG energy was calculated for the distribution of Fourier coefficients of $|\mathbf{G}|^2$-specified plane waves at symmetry points Γ, N, and H of its bcc Brillouin zone. The FLAPW−Fourier spectra thus obtained are shown in Figure 14d along with its total and Co 4p and P 3p DOSs. One can clearly see a deep pseudogap at the Fermi level in the DOS. The CG energy meets the Fermi level at $|\mathbf{G}|^2 = 26$ corresponding to symmetry points N of its Brillouin zone. The *critical* $|\mathbf{G}|_c^2 = 26$ is found to coincide well with $(2k_F)^2 = 26.24$ derived from the Hume-Rothery plot in Figure 14c. This is nothing but a demonstration of the fulfillment of the interference condition $(2k_F)^2 = |\mathbf{G}|_c^2$ for CoP_3. This means that the origin of the pseudogap at the Fermi level can be interpreted in terms of the interference condition. The value of e/a is deduced to be 4.40 by inserting the $(2k_F)^2$ obtained above into eq 9. It is of great importance to mention that the *critical* $|\mathbf{G}|_c^2 = 26$ is commonly found for a family of 10 skutterudite compounds TMP_3 (TM = Co, Ni, Rh, and Ir), $TMAs_3$ (TM = Co, Rh, and Ir), and $TMSb_3$ (TM = Co, Rh, and Ir; cI32). This was taken as an evidence that all of them obey the Hume-Rothery electron concentration rule with e/a = 4.34 ± 0.20[26] and that the Hume-Rothery stabilization mechanism holds for such pseudogap-bearing polar compounds with a covalency of 60% and an ionicity of 15%.

4.3.2. TM_3P (TM = Cr, Mn, Fe, and Ni; tI32) Compounds. Among the many P-based intermetallic compounds studied in the present work, we will show below that four TM_3P (TM = Cr, Mn, Fe, and Ni; tI32) compounds obey the Hume-Rothery electron concentration rule with e/a = 2.20 ± 0.20. Parts a and b of Figure 15 summarize the TH−HR data and their NFE curves for TM_3P (TM = Cr, Mn, Fe, and Ni) compounds, respectively. Because of the presence of a huge anomaly due to TM 3d states across the Fermi level in Figure 15a, one can hardly expect the e/a = constant rule to hold in this family on the basis of the local reading method. The construction of the NFE curve is indispensable. As shown in Figure 15b, the resulting NFE curves fall on an almost universal curve, and as a result, the value of $(2k_F)^2$ turns out to be almost 16.5 for the four tI32 compounds.

Parts a−d of Figure 16 show the FLAPW−Fourier spectra for the TM_3P (TM = Cr, Mn, Fe, and Ni) compounds, respectively. The spectra were calculated at symmetry points Γ, N, X, Z, and P in the Brillouin zone of the body-centered-tetrahedral (bct) structure. The energy dependence of the square of the Fourier coefficients is shown for Cr_3P, as marked with gray bars for each $|\mathbf{G}|^2$-specified wave in Figure 16a. The CG energy is calculated by taking its intensity-weighted average and marked with colored circles. For simplicity, only the $|\mathbf{G}|^2$ dependence of the CG energy is plotted in Figure 16b−d along with the total and TM 4p and P 3p partial DOSs and the NFE curves reproduced from Figure 15b.

The *critical* $|\mathbf{G}|_c^2$ is found to be distributed at around a constant value of 16.5 at symmetry points N for all four compounds. [The *critical* $|\mathbf{G}|_c^2 = [2\pi/(a^2c)^{1/3}]^2[(c/a)^{2/3}(h^2 + k^2) + (a/c)^{4/3}l^2]$ becomes noninteger in units of $\{2\pi/(a^2c)^{1/3}\}^2$ for the bct structure.] Although the total DOS do not show a pseudogap structure in Ni_3P, we consider it to be hidden behind the TM d states. The p states are pushed to the bottom and top of the d band as a result of d-state-mediated splitting.[19−25] As marked by a red arrow, the minimum of a pseudogap in the p states is always found near the Fermi level. From the analysis above, we conclude that a constant e/a = 2.20 ± 0.20 rule holds for all of these tI32 compounds.

It is interesting to examine to what extent the e/a value derived for each tI32 compound agrees with that obtained from a composition average of e/a of constituent elements: $(e/a)_{Cr} = 0.92$, $(e/a)_{Mn} = 1.05$, $(e/a)_{Fe} = 1.05$, and $(e/a)_{Ni} = 1.16$. The e/a values for Cr_3P, Mn_3P, Fe_3P, and Ni_3P turn out to be 1.97, 2.07, 2.07, and 2.15, respectively, in good agreement with the e/a = 2.20 rule discussed above within ±10%. As noted earlier, $(e/a)_{Ni} = 1.16$ obtained in relation to Figure 9c is not consistent with $(e/a)_{Ni} = 0.0$ deduced from the Ni concentration dependence for Al-rich Al−Ni alloy systems.[24] Further work may be needed to explore the environmental effect on e/a for Ni and its compounds, possibly including Pd, Pt, and their compounds.[24,25] Putting it aside, we can safely say that confirmation of the e/a = 2.20 rule for the TM_3P (tI32) compounds across a wide group of TM 3d elements of the Periodic Table justifies our claim that e/a values for most of the TM elements of the Periodic Table are distributed in the vicinity of unity and that these FLAPW-derived e/a data should be used upon handling of the e/a issue on TM-containing alloys and compounds in place of those proposed by Raynor[13] and Pauling[14] many years ago.

4.4. Interference Condition for Pseudogap- or True-Gap-Bearing P Compounds. Regardless of whether the TM element is involved and orbital hybridization effects are strong or not, we have so far demonstrated the fulfillment of the interference condition and the validity of the Hume-Rothery stabilization mechanism by constructing a plot of e/uc, i.e., the number of electrons per unit cell, which is equivalent to $(2k_F)^2$, versus the *critical* reciprocal lattice vector $|\mathbf{G}|_c^2$ for a large number of pseudogap-bearing compounds.[19,20,25,27,28] In the present work, we have studied how the e/a determination is influenced by the ionicity and covalency. Thus, we consider it to be timely to examine whether the interference condition still holds or fails when the ionicity is increased beyond 50%.

Figure 17 shows the e/uc versus $|\mathbf{G}|_c^2$ plot for P-based compounds studied in the present work. It is clear that all of the data points, regardless of the degree of covalency and ionicity involved, fall on the NFE line with a slope of $^3/_2$ previously established for the data reported in the literature.[19,20,25,27,28] Even the A−P compounds with ionicity exceeding 55%, where the e/a determination becomes unstable, are found almost on the line. This demonstrates that the NFE model can be successfully applied and the origin of a pseudogap and true gap at the Fermi level universally discussed in terms of the interference condition.

5. CONCLUSIONS

We have performed first-principles FLAPW−Fourier band calculations for four pure elements, P, As, Sb, and Bi, in group 15 and as many as 59 intermetallic compounds formed by combining P in group 15 with elements from alkali metals Li, Na, K, Rb, and Cs in group 1 up to Si and Ge in group 14 of the Periodic Table. We aimed at investigating the effect of the ionicity and covalency on the e/a determination of compounds and to what extent the Hume-Rothery stabilization mechanism is validated when the ionicity is increased.

The van Arkel−Ketelaar triangle with vertices designated as metallic (M), ionic (I), and covalent (C) was constructed using

dx.doi.org/10.1021/ic502286q | Inorg. Chem. 2015, 54, 930−946

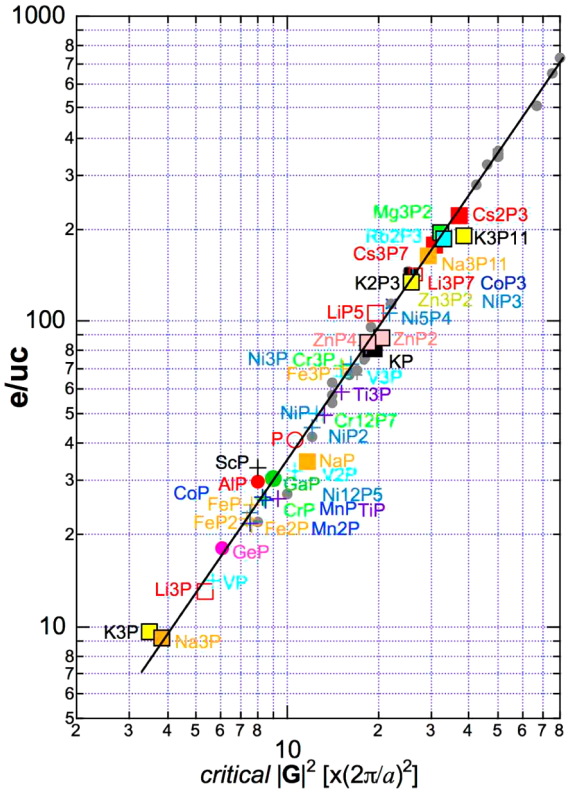

Figure 17. e/uc versus $|G|_c^2$ diagram on a log−log scale for P-based compounds with a pseudogap or true gap across the Fermi level. The square of the *critical* reciprocal lattice vector $|G|_c^2$ is expressed in units of $(2\pi/a)^2$ in the cubic system. Small gray circles represent the data reported earlier in the literature.[19,20,25,27,28] The NFE line with a slope of $^3/_2$ (black) can be universally drawn for all compounds, regardless of the chemical types of the bonds involved. Note that the interference condition $(2k_F)^2 = |G|_c^2$ is rewritten as e/uc = $(\pi/3)[|G|_c^2]^{3/2}$.

a separation energy or an energy difference between the CG energies of FLAPW-derived s and p partial DOSs as a measure of the covalency and the Allen electronegativity difference as a measure of the ionicity. All P-based intermetallic compounds fall in a narrow, vertically extended strip with 30−60% covalency, 10−64% ionicity, and 5−30% metallicity in the triangle map shown in Figure 1. The values of $(2k_F)^2$ and e/a can be safely determined and the Hume-Rothery stabilization mechanism discussed in terms of the interference condition for all P-based compounds as long as the ionicity is lower than 50%. The determination of both $(2k_F)^2$ and e/a becomes unstable in A−P (A = Li, Na, K, Rb, and Cs) compounds, where ionicity exceeds 50%. Two new Hume-Rothery electron concentration rules have been theoretically confirmed in TM_3P (TM = Cr, Mn, Fe, and Ni) compounds with e/a = 2.20 and 10 skutterudite compounds TMP_3 (TM = Co, Ni, Rh, and Ir), $TMAs_3$ (TM = Co, Rh, and Ir), and $TMSb_3$ (TM = Co, Rh, and Ir; cI32) with e/a = 4.34.

Finally, the FLAPW−Fourier-derived e/a values of pure elements of the Periodic Table are summarized in Figure 18. Among them, elements in period 3 from K to Zn were studied in ref 24 and those in periods 4 and 5 from Rb to Cd and from Cs to Au in ref 25, Be in ref 21, Ca and Cd in ref 22, Zn, Y, and Sc in ref 23, and Zn, Li, Na, Mg, Al, Ga, Ge, Sn, and Pb in refs 27 and 28. The remaining elements Si, Hg, and Tl were studied in the present work.

AUTHOR INFORMATION

Corresponding Author

*E-mail: uichiro@sky.sannet.ne.jp. Phone and fax: +81-52-823-3500.

Notes

The authors declare no competing financial interest.

ACKNOWLEDGMENTS

U.M. is grateful for financial support of the Grant-in-Aid for Scientific Research (Contract 26420668) from the Japan Society for the Promotion of Science. He is also indebted to Prof. Masashi Hasegawa and Dr. Yuichi Shirako, Nagoya University, for valuable discussions and for providing him literature information about works by Allen on the construction of the van Arkel−Ketelaar triangle.

REFERENCES

(1) Hume-Rothery, W. *J. Inst. Met.* **1926**, *35*, 295−361.
(2) Westgren, A.; Phragmén, G. *Z. Metallkd.* **1926**, *18*, 279−284.
(3) Westgren, A.; Phragmén, G. *Z. Anorg. Chem.* **1928**, *175*, 80−89.
(4) Westgren, A.; Phragmén, G. *Metallwirtschaft* **1928**, *7*, 700−703.
(5) Westgren, A.; Phragmén, G. *Trans. Faraday Soc.* **1929**, *25*, 379−385.

e/a of elements in the periodic table

1	2											13	14	15
Li 1.02	Be 2.19											B	C	N
Na 1.00	Mg 2.02	3	4	5	6	7	8	9	10	11	12	Al 3.01	Si 4.00	P 5.12
K 1.00	Ca 2.00	Sc 2.94	Ti 0.92	V 0.76	Cr 0.92	Mn 1.05	Fe 1.05	Co 1.11	Ni 1.16	Cu 1.00	Zn 2.04	Ga 3.00	Ge 4.00	As 4.92
Rb 1.00	Sr 1.89	Y 3.15	Zr 0.81	Nb 0.51	Mo 0.83	Tc 0.88	Ru 1.00	Rh 0.92	Pd 0.0	Ag 1.00	Cd 2.02	In 3.00	Sn 4.00	Sb 5.00
Cs 1.05	Ba 2.10	La 2.90	Hf 1.23	Ta 0.99	W 1.29	Re 1.31	Os 1.49	Ir 1.58	Pt 0.0	Au 1.00	Hg 1.87	Tl 3.00	Pb 4.00	Bi 4.97

Figure 18. Electrons per atom ratio, e/a, of elements of the Periodic Table so far evaluated from the FLAPW−Fourier analysis including the present work. The value of e/a = 2.24 was reported for Be, using the local reading method.[21] The data for Be was newly reevaluated by applying the NFE method to suppress anomalies caused by a pseudogap across the Fermi level.

dx.doi.org/10.1021/ic502286q | *Inorg. Chem.* 2015, 54, 930−946

(6) Hume-Rothery, W.; Mabbott, G. W.; Channel-Evans, K. M. *Philos. Trans. R. Soc., A* **1934**, *233*, 1−97.
(7) Mizutani, U. *Hume-Rothery Rules for Structurally Complex Alloy Phases*; CRC Press, Taylor & Francis Group: Boca Raton, FL, 2010.
(8) Mott, N. F.; Jones, H. *The Theory of the Properties of Metals and Alloys*; Clarendon Press: Oxford, U.K., 1936; Dover Publications Inc.: New York, 1958.
(9) Tsai, A.-P.; Inoue, A.; Masumoto, T. *Jpn. J. Appl. Phys.* **1988**, *27*, L1587−L1590.
(10) Tsai, A.-P.; Inoue, A.; Yokoyama, Y.; Masumoto, T. *Mater. Trans., JIM* **1990**, *31*, 98−103.
(11) Yokoyama, Y.; Tsai, A.-P.; Inoue, A.; Masumoto, T.; Chen, H. S. *Mater. Trans., JIM* **1991**, *32*, 421−428.
(12) Tsai, A.-P. *J. Non-Cryst. Solids* **2004**, *334*−*335*, 317−322.
(13) Raynor, G. V. *Prog. Met. Phys.* **1949**, *1*, 1−76.
(14) Pauling, L. *Phys. Rev.* **1938**, *54*, 899−904.
(15) Fujiwara, T. *Phys. Rev. B* **1989**, *40*, 942−946.
(16) Roche, S.; Fujiwara, T. *Phys. Rev. B* **1998**, *58*, 11338−11343.
(17) Krajci, M.; Windisch, M.; Hafner, J.; Kresse, G.; Mihalkovic, M. *Phys. Rev. B* **1995**, *51*, 17355−17382.
(18) Inukai, M.; Zijlstra, E. S.; Sato, H.; Mizutani, U. *Philos. Mag.* **2011**, *91*, 4247−4263.
(19) Mizutani, U.; Inukai, M.; Sato, H.; Zijlstra, E. S. *Philos. Mag.* **2012**, *92*, 1691−1715.
(20) Mizutani, U.; Inukai, M.; Sato, H.; Zijlstra, E. S. *Chem. Soc. Rev.* **2012**, *41*, 6799−6820.
(21) Sato, H., Inukai, M., Zijlstra, E. S.; Mizutani, U. Aperiodic Crystals. In *Proceedings of Aperiodic 2012*; Schmid, S., Withers, R. L., Lifshitz, R., Eds.; Springer: Heidelberg, Germany, 2013; Chapter 13, p95.
(22) Mizutani, U.; Inukai, M.; Sato, H.; Nozawa, K.; Zijlstra, E. S. Aperiodic Crystals. In *Proceedings of Aperiodic 2012*; Schmid, S., Withers, R. L., Lifshitz, R., Eds.; Springer: Heidelberg, Germany, 2013; Chapter 14, p101.
(23) Mizutani, U.; Inukai, M.; Sato, H.; Zijlstra, E. S. Aperiodic Crystals. In *Proceedings of Aperiodic 2012*; Schmid, S., Withers, R. L., Lifshitz, R., Eds.; Springer: Heidelberg, Germany, 2013; Chapter 15, p109.
(24) Sato, H.; Inukai, M.; Zijlstra, E. S.; Mizutani, U. *Philos. Mag.* **2013**, *93*, 3029−3061.
(25) Mizutani, U.; Sato, H.; Inukai, M.; Zijlstra, E. S. *Philos. Mag.* **2013**, *93*, 3353−3390.
(26) Mizutani, U.; Sato, H.; Inukai, M.; Zijlstra, E. S. *Acta Phys. Pol. A* **2014**, *126*, 531−534.
(27) Mizutani, U.; Sato, H.; Inukai, M.; Zijlstra, E. S.; Lin, Q.; Corbett, J. D.; Miller, G. J. *Acta Phys. Pol. A* **2014**, *126*, 535−538.
(28) Mizutani, U.; Inukai, M.; Sato, H.; Zijlstra, E. S.; Lin, Q. *Philos. Mag.* **2014**, *94*, 2571−2594.
(29) Nesper, R. *Prog. Solid State Chem.* **1990**, *20*, 1−15.
(30) Allen, L. C.; Capitani, J. F.; Kolks, G. A.; Sproul, G. D. *J. Mol. Struct.* **1993**, *300*, 647−655.
(31) Allen, L. C. *J. Am. Chem. Soc.* **1989**, *111*, 9003−9014.
(32) http://en.wikipedia.org/wiki/Electronegativity, last accessed on Nov 3, 2014.
(33) Blaha, P.; Schwarz, K.; Madsen, G.; Kvasnicka, D.; Luitz, J. Available at http://www.wien2k.at/, last accessed on Nov 3, 2014.
(34) Villars, P. *Pearson's Handbook*; ASM International: Materials Park, OH, 1997.
(35) Okamoto, H. *Phase Diagrams for Binary Alloys*; ASM International: Materials Park, OH, 2000.